AN ABSTRACT OF THE THESIS OF

Michael Kenneth Gaughan (Name) for the degree of Doctor of Philosophy (Degree)

in Oceanography (Major) presented on December 19, 1975 (Date)

Title: PREDICTION OF BREAKER TYPE AND MEASUREMENT OF SURF-BORES ON AN OCEAN BEACH

Abstract approved: Redacted for privacy
Paul D. Komar

This study applies the theory of wave propagation in water of gradually varying depth, as developed by Biesel (1952), to determine the dependence of spilling and plunging breaker types on the beach slope tangent s and on the deep water wave steepness H_∞/L_∞, the ratio of the deep water wave height H_∞ to the deep water wave length L_∞. The impetus for the study is that the dissipation of energy and the transfer of momentum by the waves to the nearshore water significantly depends on the breaker type. By representing the fluid motion at the surface in Lagrangian coordinates, a graph is developed for the breaker type based on 21 combinations of s and H_∞/L_∞. A comparison with laboratory wave data shows good agreement with this graph based entirely on theory. The steepening of the shoaling wave profile on the shoreward wave face leads to the occurrence of a vertical surface, a natural breaking criterion. The dimensionless ratios H_b/H_∞ and H_b/h_b, where H_b is the breaker height and h_b the depth at breaking, are theoretically evaluated and compared to observations.

In addition, this study investigates waves and breakers found in

the surf zone of a gently sloping (s = 0.007) sand beach at Agate Beach, Oregon. By recording the local water surface elevation simultaneously at two positions located along an onshore-offshore line while also taking time-lapse (one photo per second) photography, it was found that surf waves could be classified into four types: (1) The surf-bore, characterized by a short, steep, breaking shoreward face of turbulent, air-entrained water, while the seaward side of the crest is of low slope with few air bubbles remaining from the passage of the breaking wave face. (2) The undular surf-bore which is similar to the surf-bore but has one to three small waves just seaward of the breaking wave face. (3) Steep finite amplitude unbroken waves with nearly symmetrical surface profiles about a vertical plane through the crest. (4) Incipient breakers, formed when the unbroken waves of type-3 finally become unstable and break, usually forming spilling breakers. These four types of surf waves can be identified in recordings of the water surface elevation with wave staffs. Each give characteristic profile traces. These identifications are confirmed by time-lapse photography. Of the four types of surf waves, the surf-bore (type-1) is most frequently measured and is most typical of the surf on low sloping beaches.

The depth parameter h_1/h_2, the ratio of the depth at the wave crest to the depth at the trough preceding the crest, was determined for over 900 individual wave observations. The surf-bore type could not be distinguished from the undular surf-bore type. However, the mean value $h_1/h_2 = 1.60$ indicates that surf-bores continue breaking due to the amplitude dispersion mechanism characteristic of finite

amplitude long waves. This implies that the breaking index H/h can vary both spatially and temporally given a spectrum of incident wave frequencies. Finally, for frequencies greater than the predominant incident wave frequency, the surface elevation spectral energy density decays exponentially with increasing frequency. A physical derivation which explains this form of the spectra is lacking.

Prediction of Breaker Type and Measurement of Surf-bores on an Ocean Beach

by

Michael Kenneth Gaughan

A THESIS

submitted to

Oregon State University

in partial fulfillment of
the requirements for the
degree of

Doctor of Philosophy

June 1976

APPROVED:

Redacted for privacy

Professor of Oceanography
in charge of major

Redacted for privacy

Dean of the School of Oceanography

Redacted for privacy

Dean of the Graduate School

Date Thesis is Presented December 19, 1975

Typed by Margie Wolski for Michael Kenneth Gaughan

ACKNOWLEDGEMENTS

I am especially grateful to my major professor, Paul Komar. His talent for perceiving the essential mechanisms in many physical and geological processes and his attention to the myriad of details encountered in scientific problems were particularly valuable to my education.

This work is a result of research sponsored in part by the Oregon State University Sea Grant College Program, supported by NOAA Office of Sea Grant, Department of Commerce, under Grant #04-6-158-44004. The U. S. Government is authorized to produce and distribute reprints for governmental purposes notwithstanding any copyright notation that may appear hereon.

TABLE OF CONTENTS

LIST OF TABLES

LIST OF FIGURES

LIST OF FIGURES, continued:

LIST OF SYMBOLS

Symbol	Meaning
a	wave amplitude in deep water
f	wave frequency
g	acceleration due to gravity
h	water depth below the still water level
h_1	water depth below bore crest
h_2	water depth below trough preceding bore crest
h_b	water depth at breaking point
H	wave height, vertical distance from trough to crest
H_∞	wave height in deep water
H_b	wave height at the breaking point
k	wave number, $2\pi/L$
L	wave length
L_∞	wave length in deep water
s	beach slope tangent
S	spectral energy density
t	time
T	wave period
u	horizontal particle velocity
u_1	horizontal particle velocity (depth averaged) at the bore crest
u_2	horizontal particle velocity (depth averaged) at the trough preceding bore crest
U_r	Ursell Number

List of Symbols, continued

Symbol	Meaning
V	bore velocity
w	vertical particle velocity
x	horizontal coordinate in direction of wave advance (positive onshore)
X	horizontal particle position in Lagrange coordinates
X_b	horizontal distance of bore crest from shoreline
z	vertical coordinate (positive upwards)
Z	vertical particle position in Lagrange coordinates
ϕ	velocity potential
ω	wave freqency, $2\pi/T$
η	free surface elevation above the still water level

PREDICTION OF BREAKER TYPE AND MEASUREMENT OF SURF-BORES ON AN OCEAN BEACH

I. PREDICTION OF BREAKER TYPE AND HEIGHT

INTRODUCTION

As ocean waves shoal and approach the shoreline they peak, become unstable, and finally break. If the beach slope is steep the wave crest curls over and plunges onto the slope ahead, the entire breaking process occurring over a relatively short horizontal distance. This type of breaker is known as the plunging breaker (Figure 1). Other waves, generally on long, low sloping beaches, become unstable slowly causing the crest to spill forward gently onto the shoreward wave face, a breaker type known as a spilling breaker (Figure 1). Spilling breaking occurs over a much larger horizontal distance than does the plunging type. A third breaker type is the collapsing breaker type which is caused by a wave-backwash interaction (Figure 1). A final breaker is the surging type (Figure 1), which occurs when the wave crest remains unbroken while the base of the shoreward wave face, with minor breaking, advances up the beach (Galvin, 1968). There is really a continuum of breaker types from spilling to plunging to surging, these categories being somewhat artificial.

The dissipation of energy and the transfer of momentum by the waves to the nearshore water may significantly depend on the breaker type. For example, relevant to the study of sediment transport by waves, the plunging breaker results in a stronger interaction with the

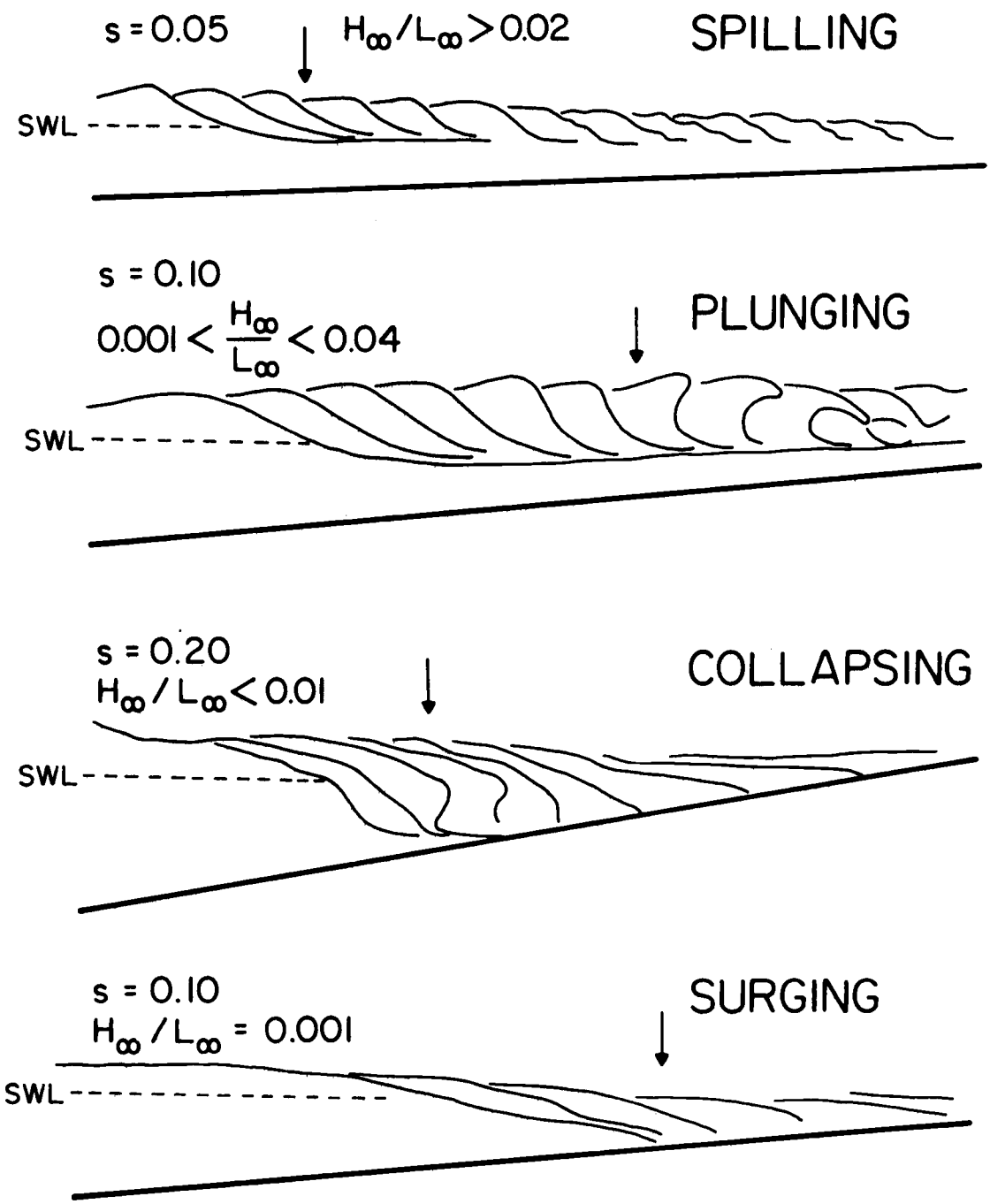

Figure 1. Principal breaker types. Position of water surface at equal time increments traced from films of waves breaking on laboratory beaches (Galvin, 1968). Arrows give breaker position.

seafloor sediments than does the spilling breaker. This has been the impetus for the study of breaker types by engineers and scientists.

Ippen and Kulin (1955), Camfield and Street (1967) and Galvin (1968) have experimentally demonstrated that the wave steepness and beach slope are key parameters which determine the breaker type. For example, the experiments of Galvin resulted in the first comprehensive quantitative classification of breaker types by relating the deep water wave steepness H_∞/L_∞ and the beach slope s to the breaker type for 43 different laboratory wave conditions.

The purpose of this study is to examine the applicability of the theory of wave propagation in water of gradually varying depth, as developed by Biesel (1952), to prediction of the breaker type for monochromatic incident waves, given the deep water wave steepness and bottom slope. This study was inspired by the results of Biesel (1952) in that he obtained solutions which bore considerable similarity to plunging and spilling breakers found on laboratory and natural beaches. A direct comparison will be made between the theoretical results and the experimental wave tank data obtained by Galvin (1968). In addition, this study will investigate the dependence of the breaker height H_b and breaker depth h_b on the deep water wave steepness. Previous relationships were based on solitary wave theory (Munk, 1949) or a modified Airy wave theory with a similarity breaking criterion (Komar and Gaughan, 1973) with the results being semi-eimpirical.

THEORY

First Order Theory

The fundamental physical relationships defining the propagation of a wave in water of gradually varying depth have been derived by Biesel (1952). His derivation is outlined here for application. The x-axis is located at mean sea level with positive x in the direction of wave propagation (onshore), and the positive z-axis is directed vertically upward as shown in Figure 2. Assuming the motion is irrotational in an incompressible fluid, a velocity potential ϕ (x,z,t) may be defined from which the velocity components are given by

$$u = \frac{\partial \phi}{\partial x} \quad , \quad w = \frac{\partial \phi}{\partial z} \tag{1}$$

where

$$\nabla^2 \phi = 0. \tag{2}$$

For small beach slope, the boundary condition at the sea floor is

$$\frac{\partial \phi}{\partial z} - s \frac{\partial \phi}{\partial x} = 0 \quad , \quad z = -h \tag{3}$$

where s is the tangent of the beach slope. The free surface boundary condition that the pressure remain constant is given by

$$\frac{\partial \phi}{\partial t} - gz = 0 \quad , \quad z = 0 \tag{4}$$

A differential equation for ϕ is obtained by differentiation of equation (4) with respect to time:

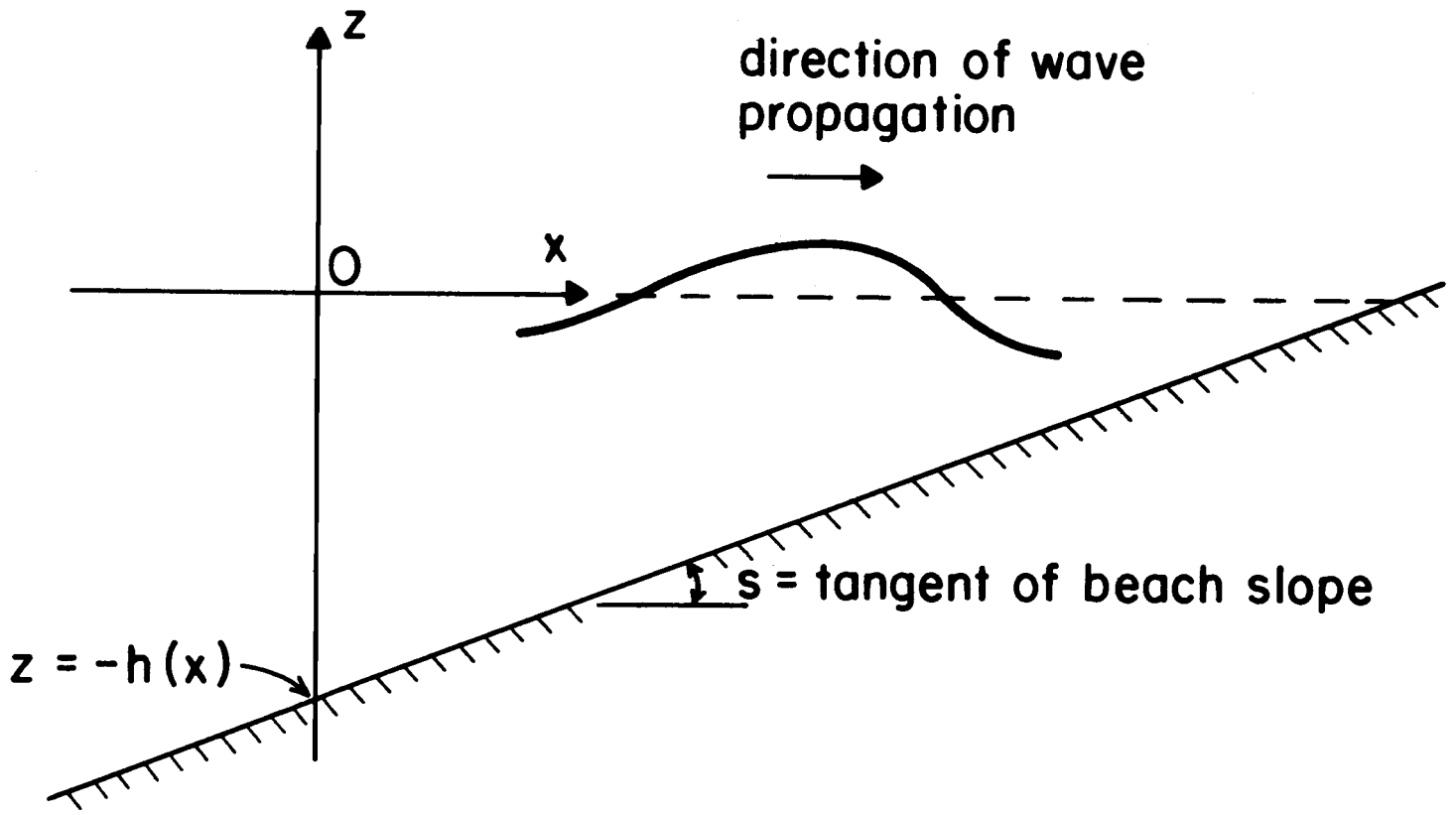

Figure 2. Coordinate system.

$$\frac{\partial^2\phi}{\partial t^2} + g\frac{\partial\phi}{\partial z} = 0 \quad , \quad z = 0. \tag{5}$$

These four conditions are satisfied to within terms of order s^2 by the function (Biesel, 1952).

$$\phi(x,z,t) = \frac{-a\omega}{k\sinh(kh)} \left[\cosh(kh + kz) \sin(\omega t - kx) \right. \tag{6}$$

$$+ s\left(\frac{kz + kh}{D^2\tanh(kh)} \sinh(kh + kz) - (kh + kz)\cosh(kh + kz) \right.$$

$$\left. \left. + \frac{k^2(z + h)^2 \cosh(kh + kz)}{D \sinh(kh) \cosh(kh)} \right) \cos(\omega t - kx) \right]$$

In this equation

$$D = 1 + \frac{kh}{\sinh(kh)\cosh(kh)} \quad , \tag{7}$$

$k = 2\pi/L$ and $\omega = 2\pi/T$, where L and T are the wave length and period, related to the water depth h through

$$gk \tanh(kh) = \omega^2 \tag{8}$$

and where

$$a = \frac{H_\infty}{2(D \tanh(kh))^{1/2}} \tag{9}$$

This velocity potential, equation (6), is used to calculate the x and z components of the displacements of the water particles whose

mean positions lie along the still water level (z = 0). This Lagrangian system of following the fluid motion is utilized because a wave shape similar to actual waves is obtained.

The calculations for the displacements are carried out according to the relationships

$$X = \int \frac{\partial \phi}{\partial x}\, dt\,, \quad Z = \int \frac{\partial \phi}{\partial z}\, dt \tag{10}$$

and yield the equations

$$X = \frac{a_\infty \sin(\omega t - kx)}{[D \tanh(kh)]^{1/2} \tanh(kh)} + \frac{s\, a_\infty \cos(\omega t - kx)}{[D \tanh(kh)]^{1/2}} \cdot \left(\frac{1 + kh \tanh(kh)}{[D \tanh(kh)]^2} + \frac{kh + 0.5(kh)^2[\tanh(kh)]^{-1}}{D \sinh(kh) \cosh(kh)} - \frac{kh}{\tanh(kh)} - 1 \right) \tag{11}$$

$$Z = \frac{a_\infty \cos(\omega t - kx)}{[D \tanh(kh)]^{1/2}} - \frac{s\, a_\infty \sin(\omega t - kx)}{[D \tanh(kh)]^{1/2}} \cdot \left(\frac{1}{D^2 \tanh(kh)} + \frac{kh}{D^2 \tanh^2(kh)} + \frac{kh[\tanh(kh)]^{-1} + 0.5\,(kh)^2}{D \sinh(kh) \cosh(kh)} - \frac{1}{\tanh(kh)} - kh \right) \tag{12}$$

From these equations the trajectories of particles along the free surface may be computed.

The instantaneous surface profile of the breaking wave may also be determined from equations (11) and (12). For a specified time the surface particle positions are calculated and plotted. These particle positions are connected by a curve which represents the wave profile. A separation distance for the mean positions must be chosen, taking into account the wave steepness and beach slope, so that adjacent instantaneous particle positions are closely spaced and yield a smooth profile.

Second Order Theory

Biesel (1952) attempted to improve the preceding theory by taking into account terms of the order H^2, the "classical" second order terms. The terms that must be added to the particle displacement equations (equations (11) and (12)) to account for this modification are, respectively,

$$X' = \frac{a_\infty^2 \, k \, [1 - 1.5 \cosh(2kh) \sinh^{-2}(kh)] \sin[2(\omega t - kx)]}{4 \, D \tanh(kh) \sinh^2(kh)} \qquad (13)$$

$$Z' = \frac{3 \, a_\infty^2 \, k \sinh(2kh) \cos[2(\omega t - kx)]}{4 \, D \tanh(kh) \sinh^4(kh)} \qquad (14)$$

These are identical to the corresponding second order terms for waves in a constant water depth (Biesel, 1952).

Breaking Criterion

The Lagrangian method of representing the fluid motion leads to a natural breaking criterion; the wave is assumed to be at the breaking point when two surface particles have the same instantaneous horizontal position. This definition is equivalent to the first occurrence of a vertical surface on the shoreward wave face (marked by arrows in Figure 1), which has been used in several laboratory experiments for some spilling and all plunging breakers [Iverson, 1952; Galvin, 1968) (data by P. D. Komar and V. P. Simmons cited by Gaughan et al., 1973)].

COMPARISON WITH LABORATORY OBSERVATIONS OF MONOCHROMATIC WAVES

The most comprehensive study of breaker types on a plane beach is that of Galvin (1968). His experiments included 43 varied laboratory conditions with beach slopes of 0.05, 0.10, and 0.20. In any laboratory experiment with oscillatory breakers it is possible for waves reflected from the beach, secondary waves (small waves of nonpermanent form which develop as a steep wave breaks down into a large wave and one or smaller waves), and backwash currents to affect the development of breaker types. Because of this, Galvin took care to see that the breaker type data satisfied the following restrictions:

1. A dominant breaker type existed. This condition was assumed satisfied when at least 70% of the waves in the steady-state sequence had the same breaker type.
2. The breaking of the large primary wave was not hindered by a

secondary wave.

The principal oscillatory breaker types obtained by Galvin are defined by tracings from film of the breaking wave profile sequence (Figure 1). Although the wave steepness in deep water is not known for the breakers in Figure 1, the range of H_∞/L_∞ which produce these breaker types for the specified slopes was determined from Galvin's Figure 3, which is an empirically determined graph of the breaker type dependence on H_∞/L_∞ and the beach slope.

Beach Slope Dependence

Figure 3 shows breaking wave profile sequences constructed from the Lagrangian equations as discussed in the previous section. The striking comparisons between the laboratory sequences and the sequences, Figure 3, based on theory indicate the validity of this approach. Figure 3 also shows the dependence of the breaker type, according to theory, on the beach slope since the wave steepness is held constant at $H_\infty/L_\infty = 0.01$. For a beach slope of $s = 0.10$ the theoretical wave profile sequence indicates a plunging breaker, and this agrees with the laboratory results in Figure 1; in this case the similarity between theoretical and observed profile changes is very noteworthy. If the beach slope is decreased to $s = 0.05$ the derived breaker type is "transitional," lying somewhere between the pure plunging and pure spilling breaker types in the continuum. Halving the slope again to $s = 0.025$ produces a derived breaker sequence that is pure spilling. Unfortunately, a comparison to actual breakers cannot be made because there are no observations of breaker types on

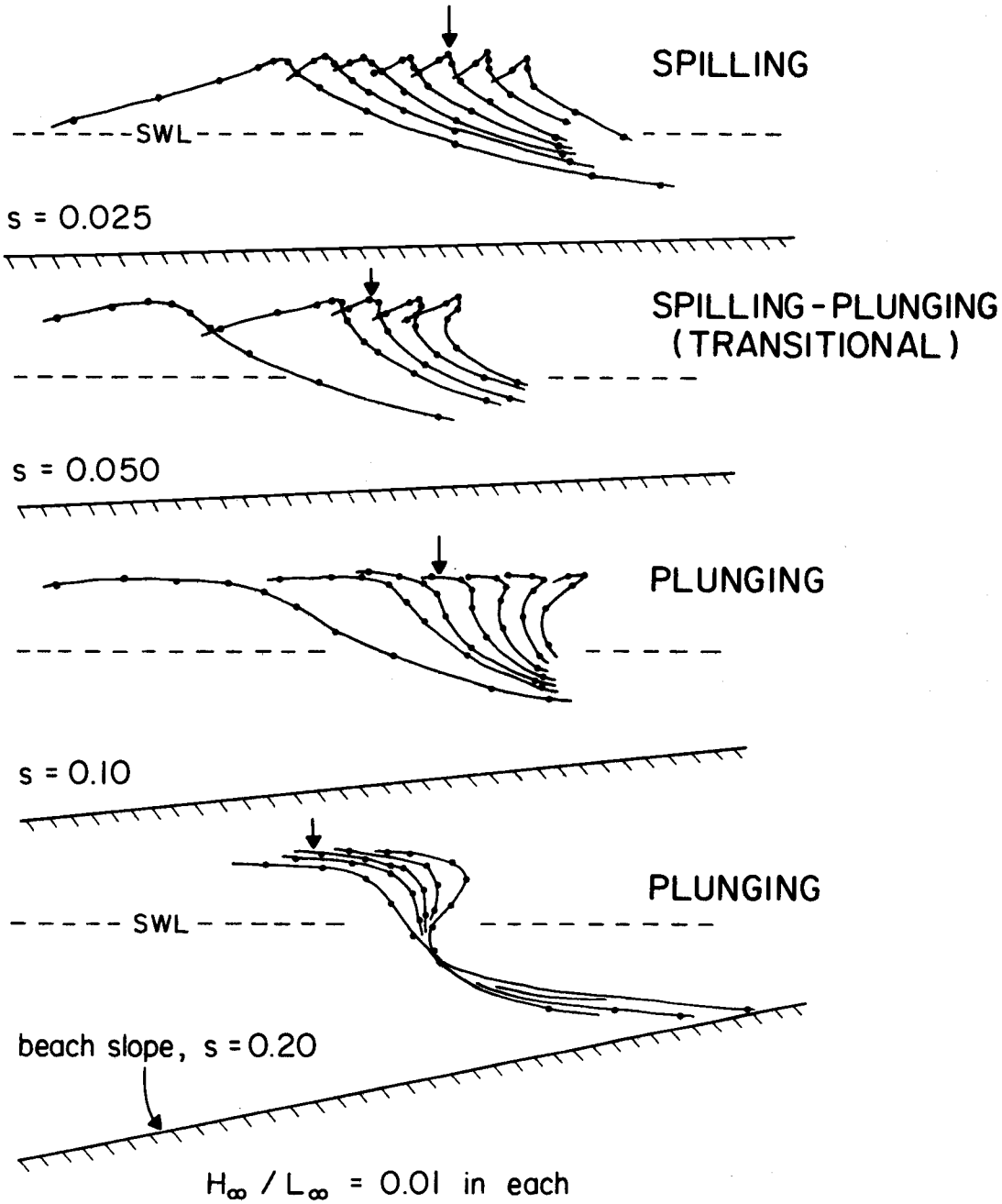

Figure 3. Wave profile sequence determined from first order theory showing dependence on the beach slope. Arrows point to breaker position.

this low slope. The theoretical results confirm the observational conclusions that a decrease in the beach slope, holding the wave steepness constant, causes the wave breaker type to change from plunging to spilling. There is agreement between theory and observation as to the range of beach slopes over which this change takes place.

Wave Steepness Dependence

In this section three examples of the breaker type's dependence on the wave steepness are illustrated. First, holding the beach slope constant ($s = 0.05$), surface profile sequences for $H_\infty/L_\infty = 0.0002$ to 0.02 is shown in Figure 4. The decrease in the deep water wave steepness produces moderate but expected changes in the breaker profiles that yield a more asymmetric and plunging type appearance to the wave. This is primarily due to the greater contrast between the seaward and shoreward facing slopes of the initially less steep wave; near the breaking position the seaward wave face is still much flatter, while the shoreward wave slope is nearly as steep especially close to the crest.

Before proceeding to additional tests of the first order theory, a comparison of the breaking wave sequences derived from second order theory to those from both first order theory and observation is made. Figure 5 shows the profiles derived from second order theory using the same wave and beach slope conditions that were applied to the first order results given in Figure 3. The general features of these second order profiles are that the waves tend to be more of the spilling variety than either those given by first order theory or by

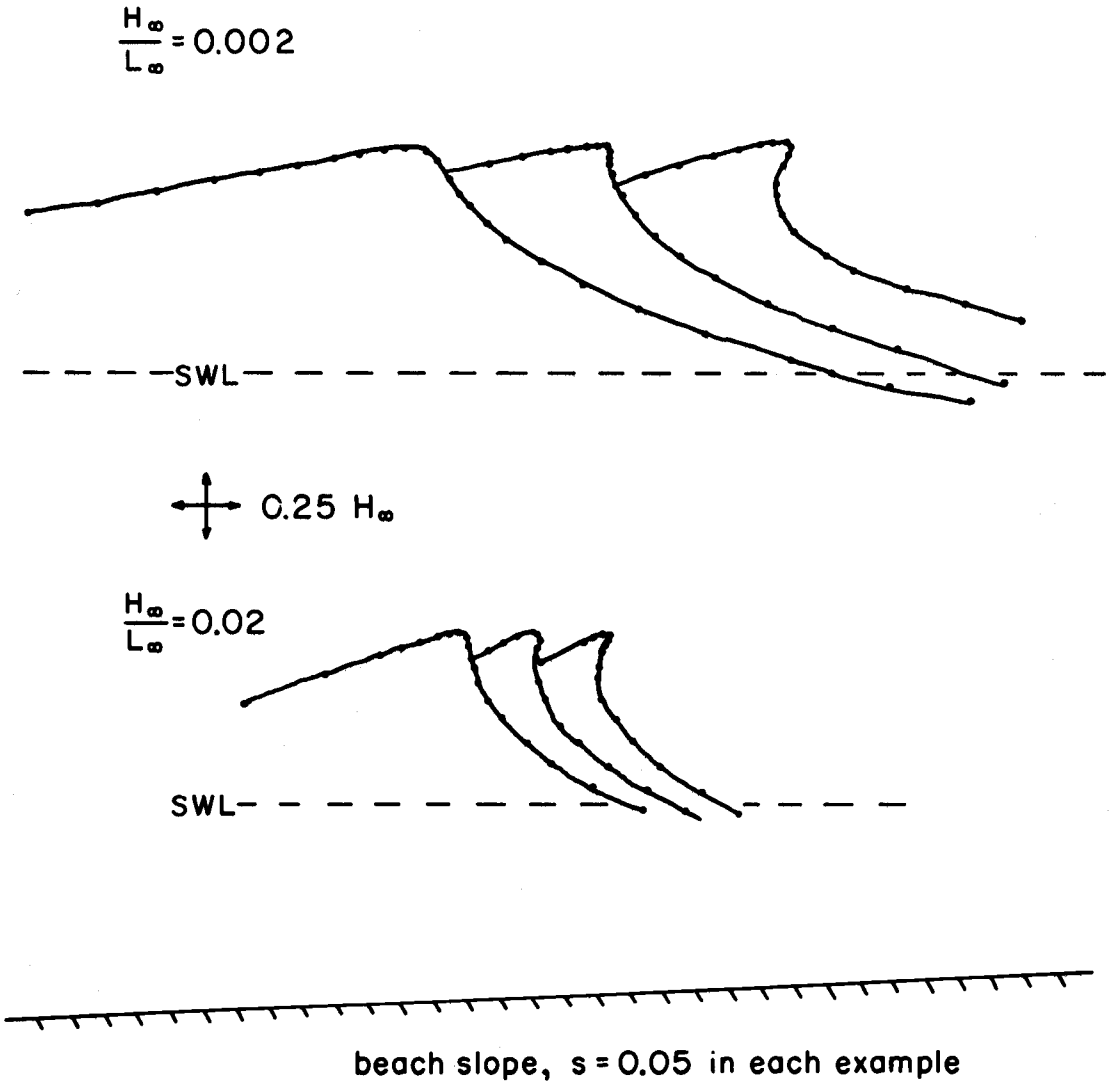

Figure 4. Wave profile sequence determined from first order theory showing dependence on wave steepness.

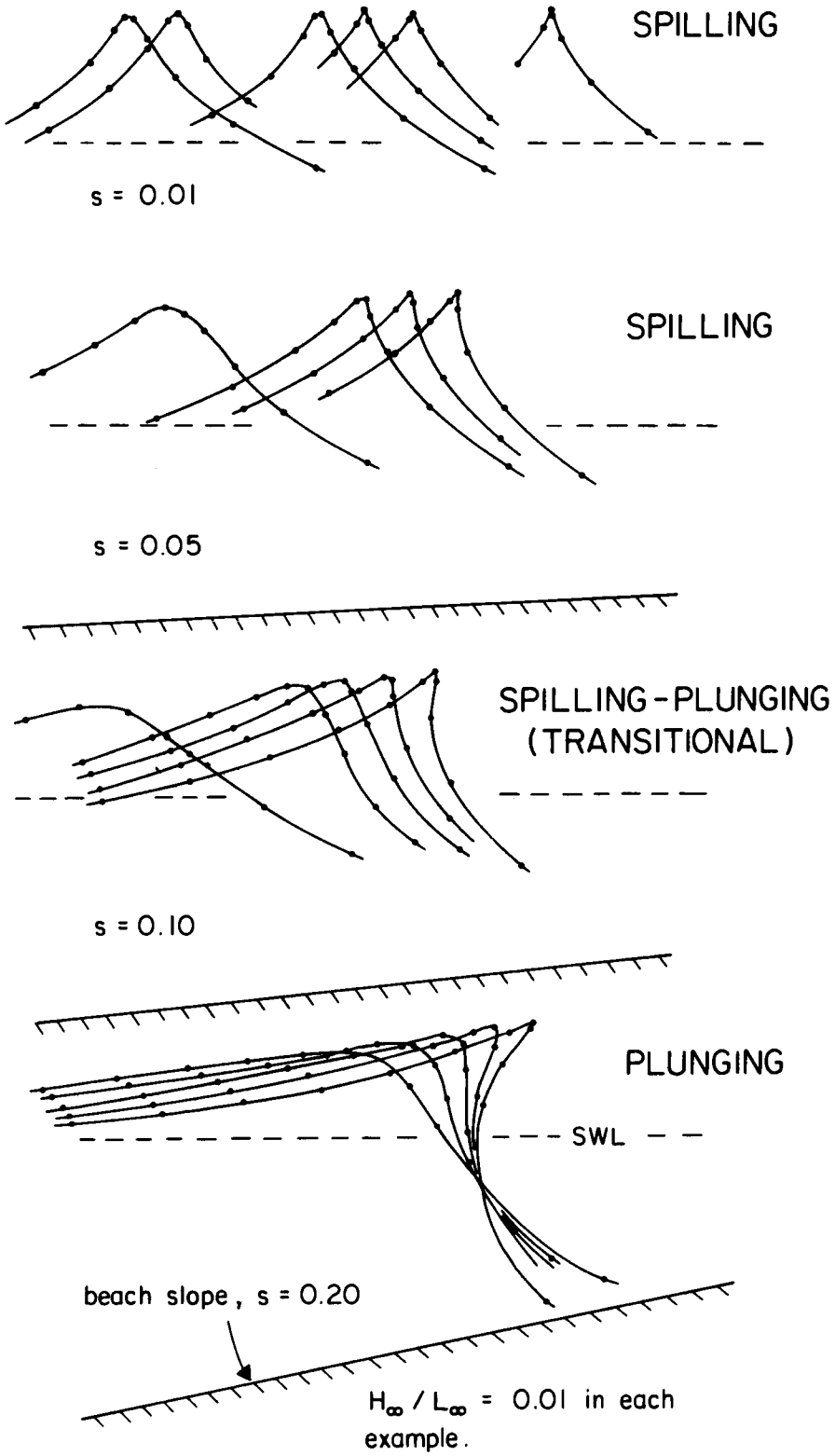

Figure 5. Wave profile sequence determined from second order theory.

observation. A plunging breaker does not occur until s = 0.20, too high a value. In addition, the breaker heights are much greater than was the case for first order theory or, as will be shown later, the observations. It is concluded that the second order theory compares less favorably with observations of breaker types than does the first order results. Therefore, second order theory will not be considered further.

Because the wave steepness for the breaker profiles of Figure 1 are only estimates, an exact comparison between film tracings and breaker profiles derived from first order theory was undertaken utilizing other data. The tracings of laboratory breakers, Figure 6A, are from films taken during a study on breaker heights and depths of breaking by Komar and Simmon (1968). For this wave breaking sequence, H_∞/L_∞ = 0.0155 and s = 0.086. The actual waves are generated in intermediate water depths so that H_∞ and L_∞ are computed quantities from $L_\infty = gT^2/2\pi$ and from an assumption of a constant energy flux, utilizing small amplitude wave theory. The time interval between breaker profiles is 1/16 second.

Figure 6B shows the derived breaker profiles for the same beach slope and H_∞/L_∞ as the observed breaker in Figure 6A. Generally, for these conditions, a comparison of the two figures demonstrates that the theory can satisfactorily predict the breaking wave profiles and therefore the breaker type. A small discrepancy between theory and observation is the premature minor breaking on the shoreward face of the actual breaker, possibly caused by instabilities induced by waves reflected from the beach or some undesirable disturbance within the

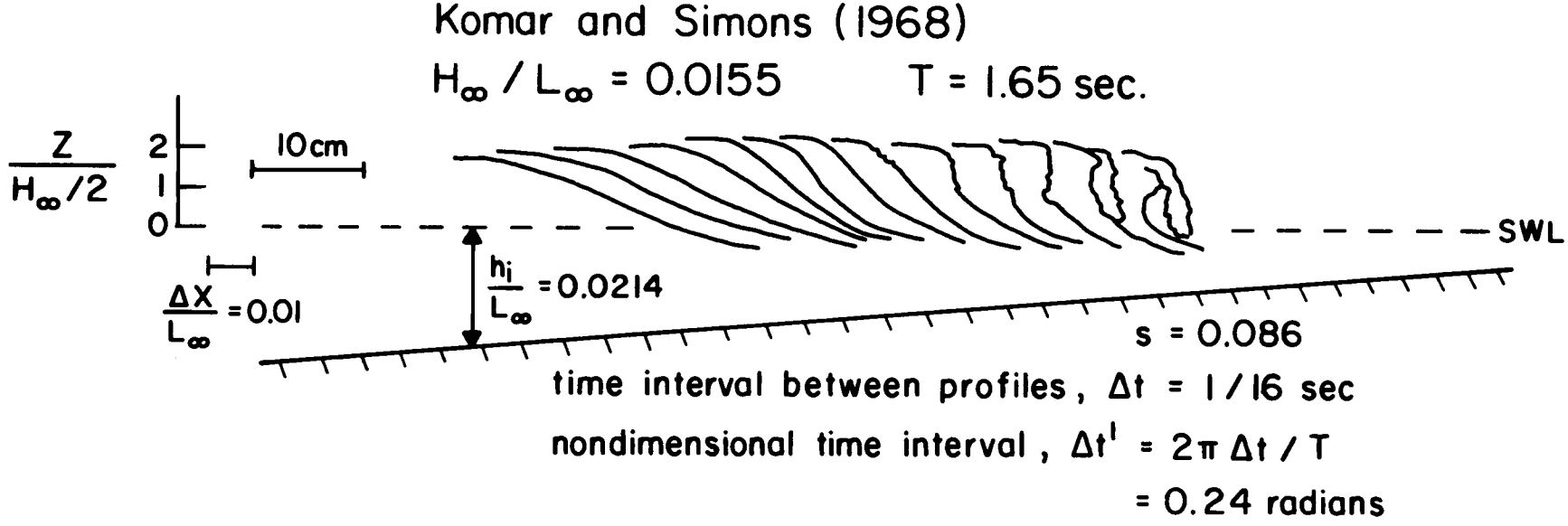

Figure 6A. Wave profile sequences from tracings of films of wave breaking on laboratory beaches (Komar and Simmons, 1968).

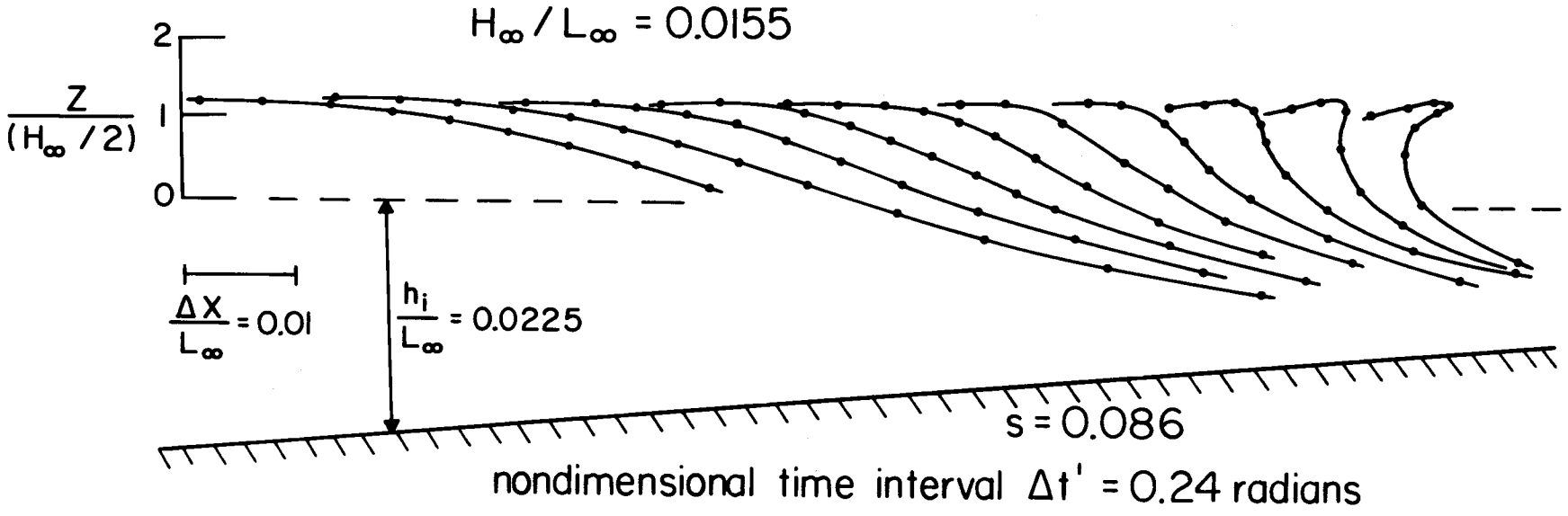

Figure 6B. Wave profile sequences determined from first order theory. Conditions correspond to those in Figure 6A.

tank. A shortcoming of the derived breaker profiles is their limited shoreward extent past the defined breaking position.

A Breaker Type Graph

In order to make a comprehensive test of the theory's capability to predict breaker types, a graph of the breaker type versus H_∞/L_∞ and s was derived by generating breaker profile sequences for a large number of conditions. These profiles were then identified as plunging, spilling, or transitional according to the accepted empirical definitions (Figure 1). The resulting graph is given in Figure 7. Individual spilling (S), plunging (P), and transition (P-S) type breakers were generated for twenty-one different conditions. According to the results based on theory, the breaker type is determined mainly by the beach slope s, changes in H_∞/L_∞ by a factor of 100 producing little effect. Because there is really a continuum of breaker types, the transition region is marked by shading instead of distinct boundary lines which suggest a discrete change in breaker type.

Two sets of data (Galvin, 1968; Komar and Simmons, 1968) are compared to the graph in Figure 8. The Komar and Simmons data were classified in an unbiased manner in that the wave period, height, and beach slope were given in code form unknown to the observer. Ten consecutive waves were classified to determine a definite breaker type. The Komar and Simmons data include observed transitional plunging-spilling breaker types.

In general, the breaker type observations, Figure 8, compare favorably with the derived breaker type dependence on beach slope and

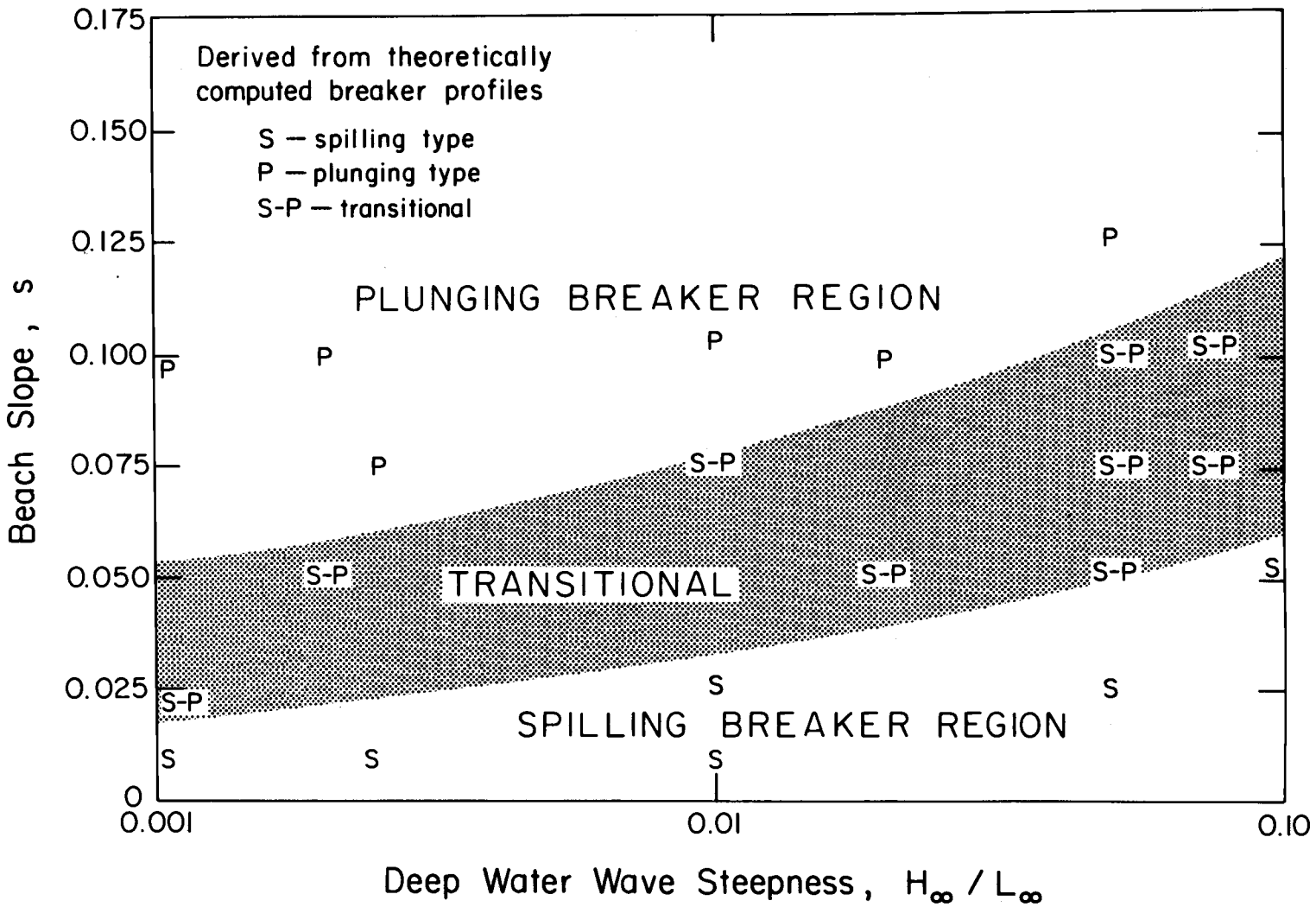

Figure 7. Graph showing breaker type dependence on deep water wave steepness and beach slope. Derived from theoretically computed breaker profiles.

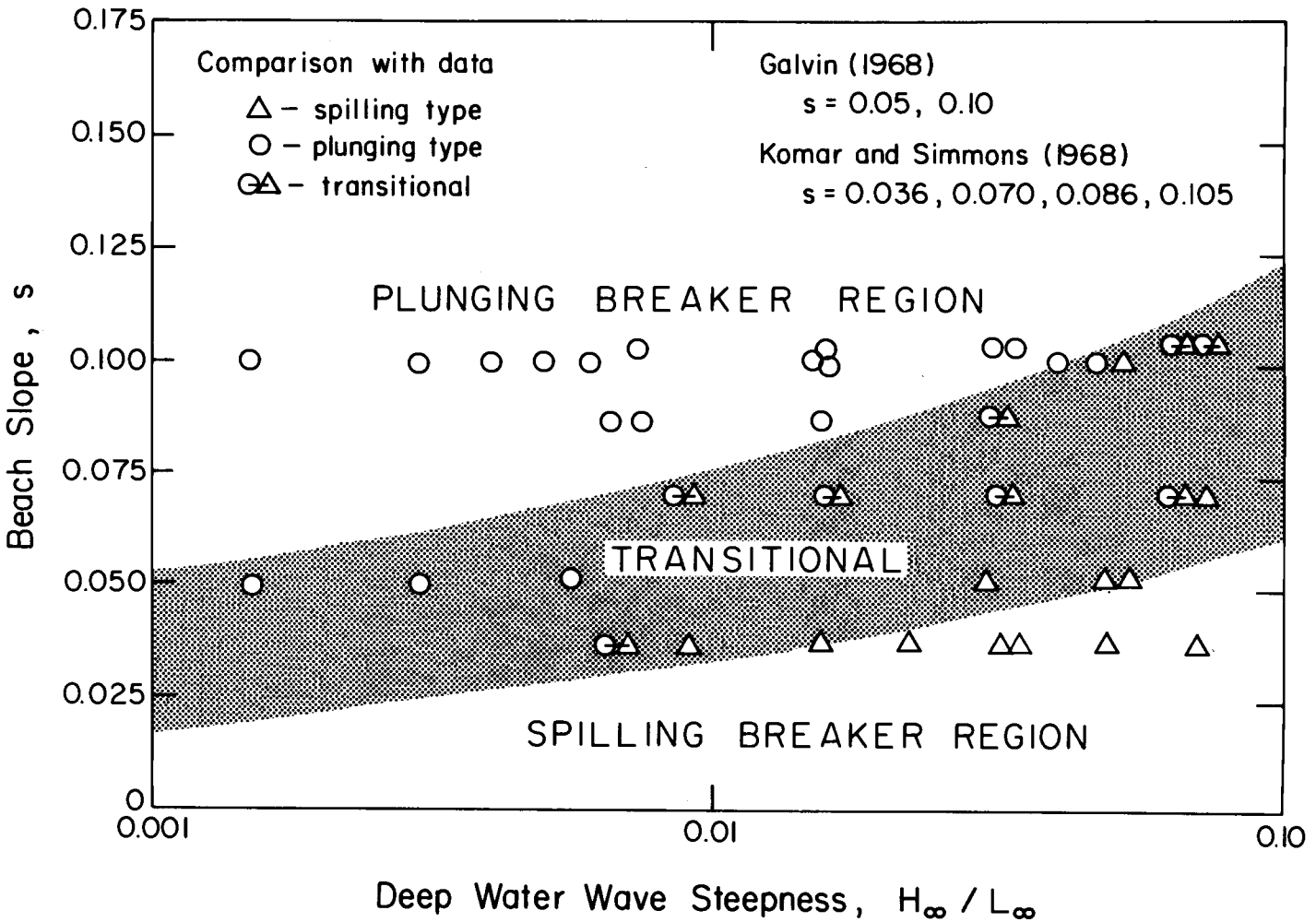

Fiugre 8. Comparison of observed laboratory breaker types to the derived graph of Figure 7.

H_∞/L_∞ . There are no spilling (plunging) breakers found in the plunging (spilling) breaker type region. The observed transitional breaker types are confined to the transitional region based on theory. The greatest disagreement occurs at low H_∞/L_∞ values where spilling breakers observed by Galvin fall into the lower transitional region. This part of the graph is poorly defined, however, so that the disagreement is minor. It can therefore be concluded again that the first order theory of Biesel (1952) gives good prediction of breaker type on a sloping beach.

Breaker Height and Depth of Breaking

Next, the ability of the theoretical development to demonstrate the dependence of the absolute values of H_b and h_b on the beach slope and deep water wave steepness is examined. For the observations H_b and h_b definitions depend on the breaker type. The spilling breaker point is the first appearance of "white water" at the crest, while the plunging breaker point is the occurrence in the breaking sequence where some part of the shoreward face of the breaker first becomes vertical (Iverson, 1952). H_b is then defined as the vertical distance between the crest at the breaker point and the spatially preceeding trough. Usually the measured breaker height is not twice the crest amplitude. For example, for the Komar and Simmons measurements, the crest is as much as three to four times the distance above the still water level as the trough is below. The breaking point for the plunging breaker corresponds to the vertical surface criterion found appropriate to the derived breaker profiles, both plunging and spilling. Careful

observations of the breaking of spilling waves may show that the shoreward face becomes vertical before the appearance of "white water."

Figure 9 tests the predicted dimensionless breaker height H_b/H_∞ versus H_∞/L_∞ against the field data of Munk (1949). The X's give the actual breaker heights determined from the theoretical approach, a smooth curve being drawn through the results. For comparison a second curve based on small amplitude wave theory and empirically fitted to the data is included (Komar and Gaughan, 1973). The curve based entirely on the theory of wave propagation in water of gradually varying depth fits the data nearly as well as the empirically fitted curve, lending credence to the theory and the applied breaking criterion. In addition to the field data of Munk (1949), the approach was tested against the laboratory data of Iverson (1952) and Komar and Simmons (1968). Again there was good agreement between theory and observation. It is concluded that the theory of Biesel (1952) for wave propagation in water of gradually varying depth gives reasonable values to the absolute value of the breaker height and shows how H_b varies with H_∞/L_∞.

A final important breaking parameter is the depth at breaking h_b. Previously the breaking criterion $H_b/h_b = 0.78$ based on solitary wave theory has been applied to shoaling oscillatory waves (Munk, 1949). This breaking criterion does not account for the changing wave profile. Figure 10 is a graph of H_b/h_b versus H_∞/L_∞ for $s = 0.05$. The theoretical points, again given as X's, lie nearly on a straight line of positive slope which increasingly deviates from the experimental wave tank laboratory values.

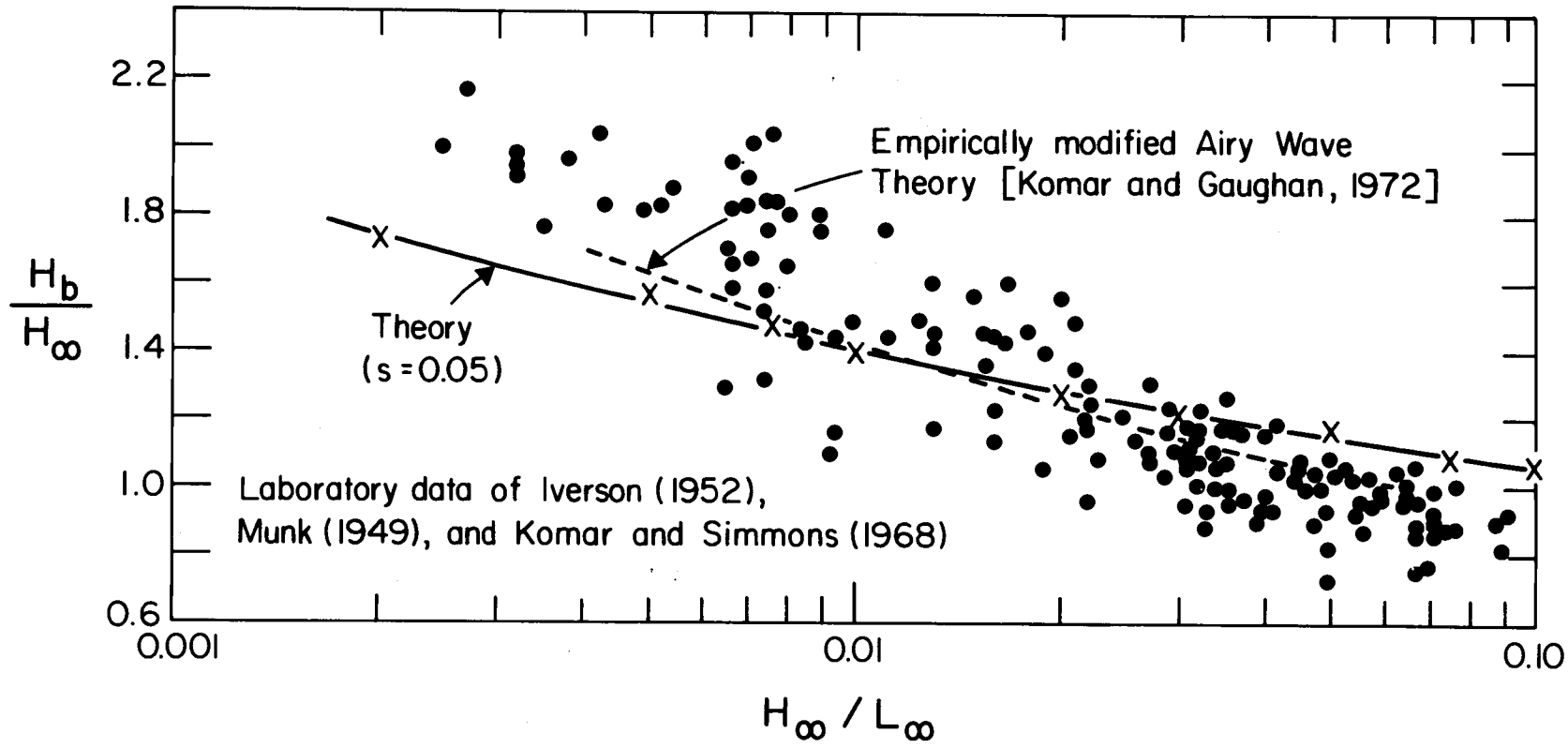

Figure 9. Wave breaker height related to deep water wave steepness. The solid curve corresponds to breaker heights determined from theoretical wave profile sequences.

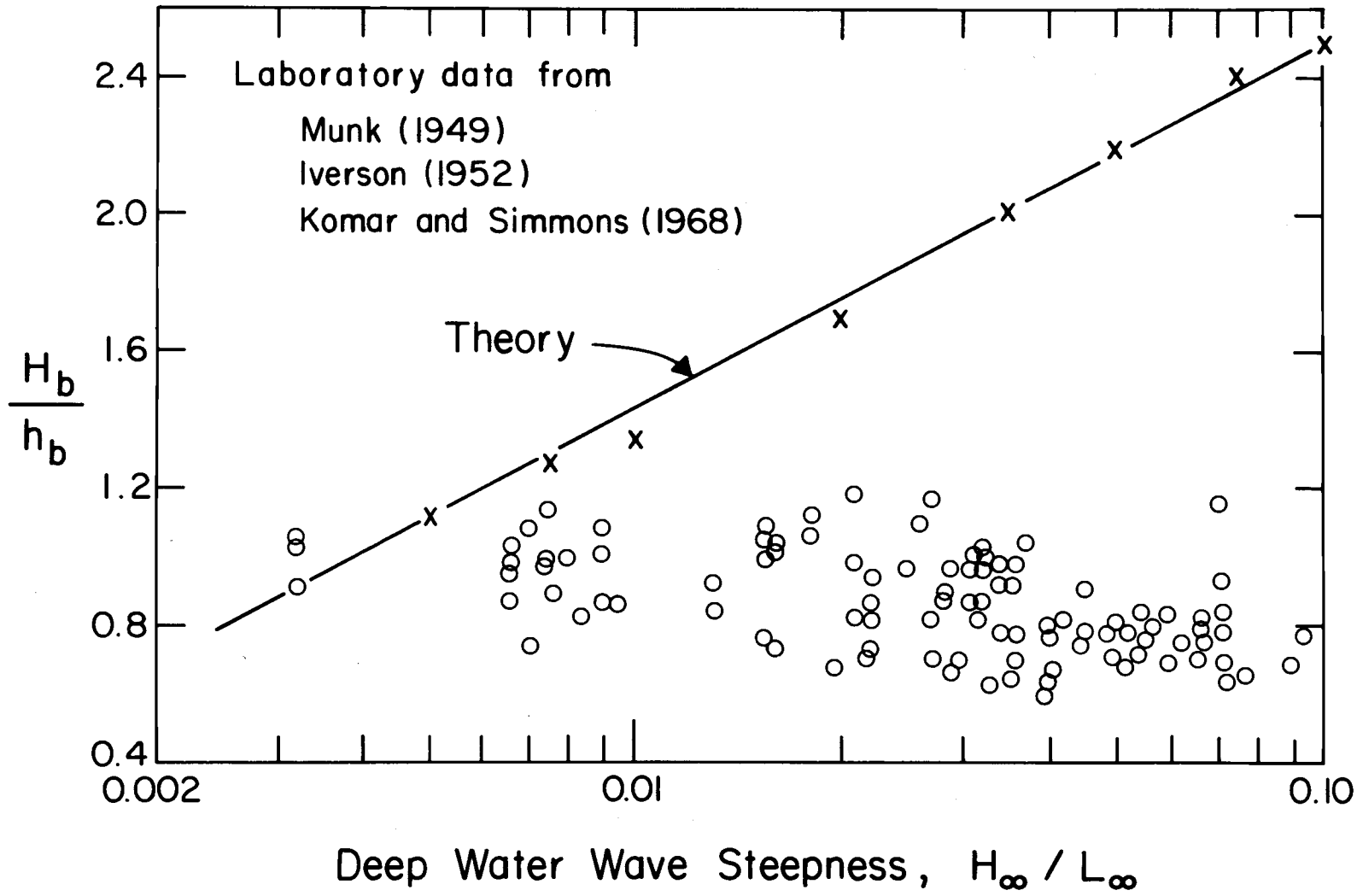

Figure 10. Breaker height to depth ratio related to the deep water wave steepness. The X symbols represent the numerical solution for s = 0.05, and for the laboratory data s = 0.033 to 0.086.

Because H_b/H_∞ is adequately predicted by the theory, the extreme H_b/h_b values must be due to the resulting h_b values being too small. That is, the predicted wave profiles travel further up the beach to shallower water before breaking than is the case with real waves. This discrepancy becomes greater with increasing wave steepness, a condition which also violates a basic assumption in the theory such that the theory is less valid for these waves of high initial steepness. This may be the cause for the poor prediction of the exact breaking position and therefore of h_b. Since the value of the wave height changes more slowly, the value of H_b would not be so dependent on the exact breaker position and that is why the values obtained for H_b with the theory are in better agreement. Another important factor is that the theoretical approach does not include the effects of the backwash, the return flow from the preceding wave. It can be expected that a backwash would cause the real wave to break sooner than it would otherwise. That is, with backwash effects the position of breaking would be shifted seaward so that the observed values of h_b would be greater than predicted by theory. Again, the effect on the value of the breaker height H_b would be to reduce H_b/h_b.

Utilizing a 120° crest angle as a breaking criterion rather than a vertical water surface would shift the breaker position seaward and thus increase h_b. Several wave series were studied in order to determine how different the results would be for this breaking criterion. Only small differences were noted, being less than 4% of the value of h_b determined using the vertical surface breaking criterion.

CONCLUSIONS

The application of the theory of wave propagation in water of gradually varying depth, as developed by Biesel (1952), to prediction of breaker type leads to the following conclusions:

1. The Langrangian method of describing the fluid motion yields breaker profile sequences (Figure 3 and 6B) that compare favorably with actual breaker profiles (Figures 1 and 6A). Also, the first occurrence of a vertical surface on the shoreward wave face appears as a natural breaking criterion compatible with previous usage in laboratory experiments.

2. Based on theoretical breaker profile sequences for 21 varied conditions of H_∞/L_∞ and beach slope s, Figure 8 yields satisfactory prediction of spilling and plunging breaker fields. The first order theory of Biesel (1952) gives a good prediction of breaker type on a sloping beach.

3. The dependence of H_b/H_∞ on H_∞/L_∞ obtained with theory fits the available data nearly as well as the proposed empirically fitted curves.

4. The value of H_b/h_b is not adequately predicted by the theory, the values being much too high. This is because the depth of breaking h_b found in the theory is too small compared to observational results. This failure is probably due to the combined limitations of the theory which does not adequately predict the breaker position, and the presence of a backwash in real oscillatory waves which causes premature breaking of the waves in somewhat deeper water.

II. MEASUREMENT OF SURF-BORES ON AN OCEAN BEACH

INTRODUCTION

One of the major subregions of the nearshore zone is the surf zone (Figure 11), commonly defined as the region in which breaking bore-like translational waves occur. These bore-like waves are the result of wave transformations which take place in the breaker zone seaward of the surf zone. In the breaker zone the waves arriving from offshore become unstable and break. During incipient breaking the crest curls over onto the shoreward wave face, either gently if the wave spills or violently if the wave plunges (see Part I of this thesis). For a plunging breaker the breaker zone is relatively narrow as the crest plunges forward and rebounds forming a breaking bore-like wave that marks the seaward limit of the surf zone. For a spilling breaker the breaker-to-bore transformation is gradual and occurs over a much wider horizontal distance. Shoreward of the surf zone is the nearshore subregion known as the swash zone (Figure 11). Within the swash zone the beach face is alternately covered by the uprush of the wave swash and exposed by the backwash. Theories which completely describe the wave transformations in these three nearshore zones are not available.

The purpose of this study is to obtain measurements of breaking waves in an ocean surf zone to test the hypothesis that initially spilling type breakers transform into surf-bores, or breaking long waves, as they travel across the surf zone. Time-lapse (one photo per second) photographs are used to develop a wave type classification

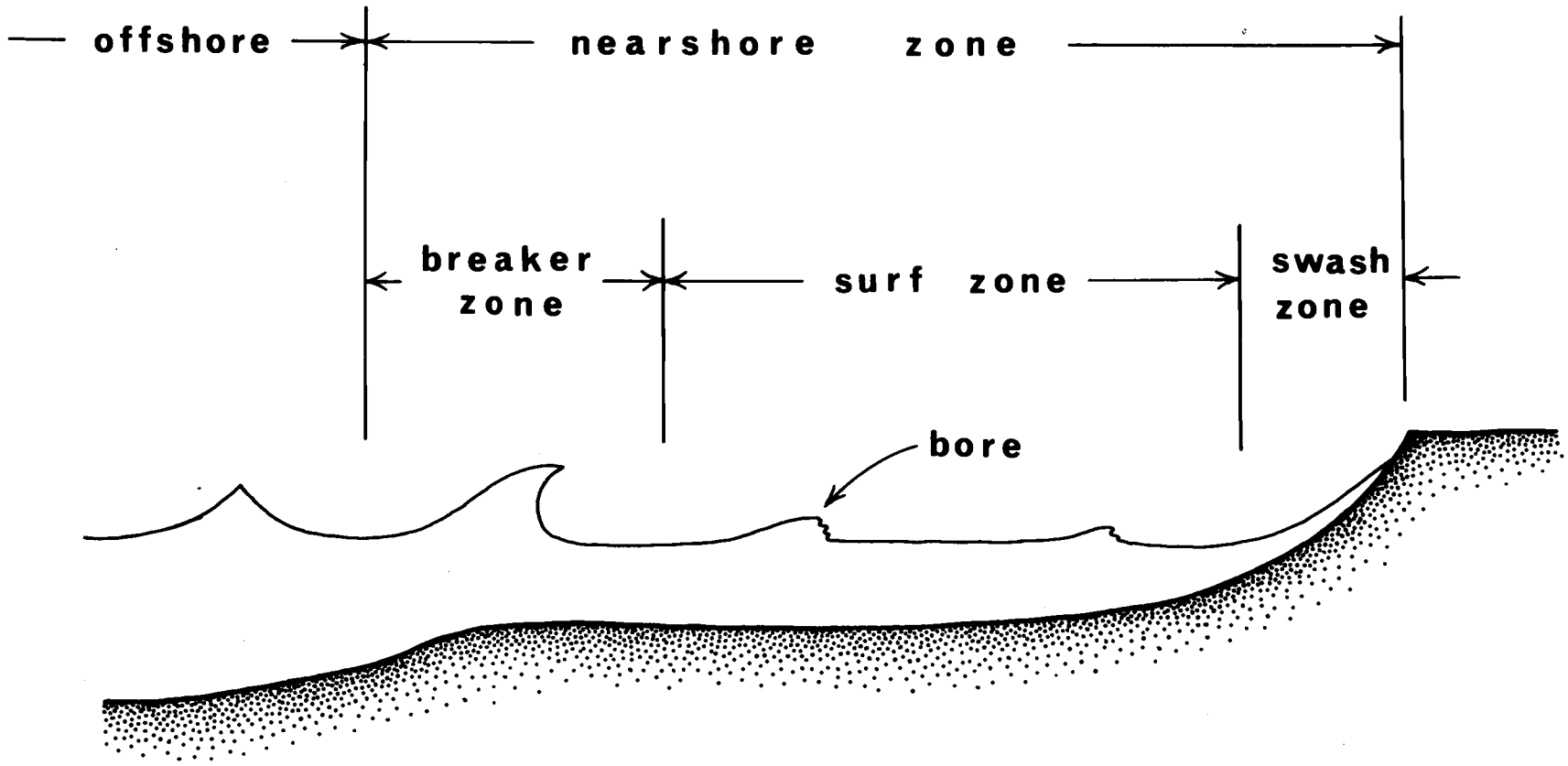

Figure 11. Sketch of the nearshore zone.

scheme for waves within surf zones. This classification is then applied to the identifiable waves on analog records of the surface elevation to show which types occur most frequently. The dimensionless depth ratio, h_1/h_2, the ratio of the depth at the wave crest to the depth immediately preceeding the crest, is measured to determine if the wave types can be quantitatively characterized. These values are then compared to h_1/h_2 values from solitary wave theory and experimental work. The previous experimental work is important because the wave systems utilized are much simpler (being either monochromatic or impulsive waves) than those encountered in the field.

Spectra are calculated from measurements of the orbital velocity associated with the passing surf-bores and from the surface elevation. The results are compared with previous field studies. These spectra describe quantitatively the spilling breaker-to-bore transformation.

WAVE THEORIES

Theoretical approaches to breaking waves in the surf zone have relied on the finite amplitude shallow water wave equations, which may be written (Peregrine, 1972)

$$\frac{\partial u}{\partial t} + u \frac{\partial u}{\partial x} + g \frac{\partial \eta}{\partial x} = 0 \qquad (15)$$

$$\frac{\partial \eta}{\partial t} + \frac{\partial}{\partial x} [(h + \eta) u] = 0 \qquad (16)$$

where η is the free surface elevation above the still water level, h is the depth below the still water level, and u is the depth-averaged horizontal particle velocity. For finite amplitude waves

obeying equations (15) and (16) in water of constant depth, it is known that the forward wave face continually steepens as the higher parts of the wave tend to overtake the preceding lower parts (Stoker, 1957). This process is termed amplitude dispersion (Peregrine, 1972). Similarly, waves on beaches of small slope continually steepen until they break, and the above equations are no longer valid within the turbulent breaking region of the wave. It is then assumed that the horizontal length of the breaking region relative to the depth is sufficiently short that the details within it may be neglected and an overall momentum and mass balance taken (Peregrine, 1972).

This assumption is termed the "bore" assumption, and the additional equations which result are

$$h_1 (u_1 - V) = h_2 (u_2 - V) \qquad (17)$$

$$h_1 u_1 (u_1 - V) + (1/2) g h_1^2 = h_2 u_2 (u_2 - V) + (1/2) g h_2^2 \qquad (18)$$

in which h_1 is the total depth behind the bore front, h_2 is the total depth in front of the bore, and V is the bore velocity (Figure 12). The velocities u_1 and u_2 are respectively depth-averaged velocities behind and in front of the bore. By using these relations and viewing the bore as a discontinuity of the wave solution, equations (15) and (16) can be used in the presence of bores (Peregrine, 1974).

It should be noted that the steep breaking region of the wave may be viewed as a moving hydraulic jump; in fact equations (17) and (18) are the continuity and momentum relationships normally applied to hydraulic jumps in open channel flow. The usual name for singular

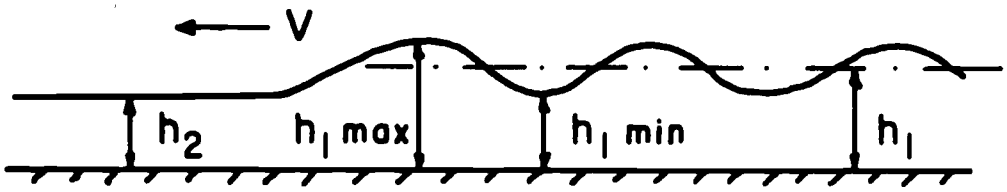

UNDULAR SURGE

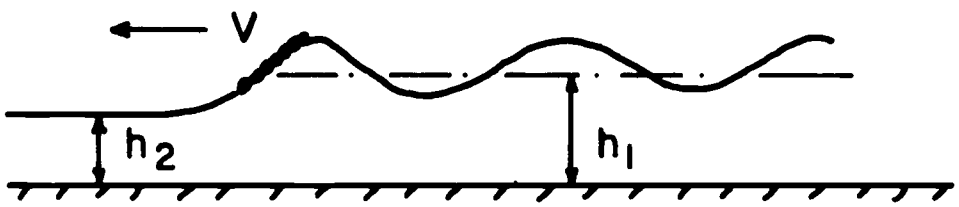

BREAKING UNDULAR SURGE

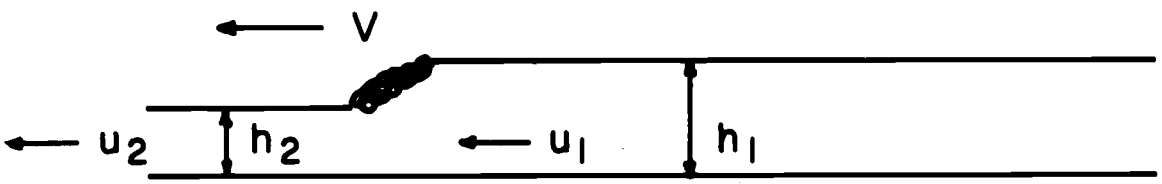

FULLY BREAKING SURGE

Figure 12. Types of surge wave profiles.

progressive long waves is 'surge.' The bore equations can be applied to breaking and non-breaking waves. They are usually chosen for breaking waves because of the complex nature of the surface elevation η ; equations (15) and (16) cannot be solved for η within the breaking region.

Once the concept of a bore is introduced all details of the flow within the breaking portion of the wave are ignored. The bore parameters which can be obtained are the bore velocity V, the distance of the bore from the shoreline, X_b, the depth behind the bore h_1 and the depth-averaged particle velocity behind the bore u_1.

The finite amplitude shallow water wave equations and the bore relationships have been utilized by several investigators to determine the properties of wave motion near the shoreline. Ho, Meyer, and Shen (1962) show that a definite similarity exists for the long wave-and-bore model even though the equations are non-linear. By non-dimensionalizing all variables (eg., velocities, surface elevation, horizontal distance, and time) by the value of the bore velocity at the shoreline and the downslope component of gravity, gs, where s is the beach slope tangent, then their model predicts that the behavior is the same for all waves and all gently sloping beaches of uniform slope. Unfortunately, the bore velocity at the shoreline (the shoreline is the intersection of the bottom slope and the still water level prior to bore arrival) is not known and must be measured.

The finite amplitude wave and bore equations have also been used to study water wave interactions in the surf zone (Peregrine, 1974). One important interaction is that between a large bore overtaking a

smaller bore in front of it. This interaction results in the formation of a single bore followed by a simple wave seaward of the bore crest.

Comments on the applicability of the finite amplitude shallow water wave and bore equations to breaking waves within surf zones are not lacking. Peregrine (1974) states that the equations should only be used quite close to the shoreline where the mean depth of water is small. Where waves have just broken or are moving shorewards as spilling breakers, Peregrine feels that the above equations are inapplicable. Meyer and Taylor (1972) comment that it is reasonable to represent a breaker as a bore when no additional information is desired. They suggest that observations indicate that bore formation precedes breaking in the sense that equations (15) and (16) are intractable over the steep unbroken shoreward wave face.

Other theoretical investigations of breakers within surf zones have relied on even more piece-meal approaches. Instead of attempting to solve the non-linear finite amplitude wave equations, Divoky, LeMehaute, and Lin (1970) assumed that spilling breakers could be modeled well with the Boussenesq steady state solitary wave theory. The breaking region of the wave was then assumed to behave as a bore.

One other class of waves deserves mention in regards to waves within ocean surf zones; these are the undular bores, or undular surges. The dissipation of wave energy through breaking is weak within undular bores, as small waves are generated at the crest by excessive horizontal pressure gradients (Peregrine, 1966). If no breaking occurs the Korteweg-deVries equations may be used to follow the development of the undular bore (Zabusky and Galvin, 1971). The

Korteweg-deVries equations may be obtained from equations (15) and (16) by the addition of the term

$$\frac{h^2}{3} \frac{\partial^3 u}{\partial x^2 \partial t}$$

to the right hand side of equation (15). Peregrine (1974) shows that this term represents the effect of the vertical velocity on both the horizontal velocity and the pressure. The small waves seaward of the bore crest are sometimes termed 'solitons.'

When considering a wave train normally incident on a sloping beach, Ursell (1952) suggested that the parameter HL^2/h^3 may be indicative of which wave theory is applicable at different distances from the shoreline prior to incipient wave breaking. In relatively deep water where HL^2/h^3 has a small value, linear wave equations are appropriate. Further inshore the crests gradually steepen and the waves appear as isolated crests. Here HL^2/h^3 is larger, and solitary or cnoidal wave theory may be applicable. Eventually HL^2/h^3 becomes even larger and the crest continually steepens until the wave breaks. Prior to breaking the finite amplitude shallow water wave equations are appropriate. After breaking one must decide if the finite amplitude wave and bore equations are the proper choice. At the present time the only other choice is the solitary wave-bore model of Divoky et al. (1970).

PREVIOUS OBSERVATIONS

Wind generated waves and swell impinging on a beach become

unstable and break, transforming into turbulent air-entrained bores which swash up the beach. During this process lower frequency wave motion may be generated such as standing waves (due to reflection of the incident waves) or edge waves. This review focuses on studies of the breaker-to-bore transformation, but observations of the lower frequency wave motion within the surf zone are also discussed.

Breaker-to-bore Transformation

Studies of the breaker-to-bore transformation are best divided into laboratory and field studies. This separation is necessary because the waves in the laboratory wave tanks do not correspond exactly to field waves for two reasons. First, they are usually sufficiently small that surface tension forces may decrease the amount of air entrained within the steep shoreward wave face. Second, the laboratory waves are either monochromatic or impulsive singular waves. This contrasts with the spectrum of wave frequencies present in the field. Because the laboratory studies utilize simpler wave systems, they are reviewed first.

Horikawa and Kuo (1967), Nakamura, Shiraishi and Sasahi (1967) and Divoky, LeMehaute, and Lin (1970) have measured the decay of breaker height on gently sloping beaches (s = 0.01) in laboratory wave tanks. Table I demonstrates that the ratio of incipient breaker height to depth at breaking, H_b/h_b, is very close to the theoretical value for maximum height solitary waves in water of constant depth (0.80). As the breakers travel shoreward of the initial breakpoint the ratio of surf-wave height H to the water depth h is less than 0.80

TABLE I. Breaker Data From Previous Laboratory Experiments

Source	Beach Slope	H_b/h_b	h/h_b:	0.90	0.80	0.70	0.60	0.50	0.40	0.30
Horikawa	0.0125	0.75-0.80	H/h:	0.56	0.51	0.46	0.44	0.46	0.47	0.53
Horikawa	0.0154	0.75-0.80	H/h:	0.59	0.56	0.53	0.53	0.54	0.56	0.61
Nakamura	0.010	0.70-0.80	H/h:	--	--	0.62	0.62	0.57	--	--
Divoky	0.0093	0.81	H/h:	0.64	0.62	0.59	0.60	0.62	0.65	0.70

over the observed range of relative depths (h/h_b = 1.0 - 0.3). This indicates that the surf-waves are no longer modeled well by the solitary wave theory; if they were, the waves would not continue to break for such low values of H/h. The Horikawa and Kuo (1967) and Divoky et al. (1970) measurements have a similar trend: H/h first decreases, reaching a minimum at a relative depth of approximately h/h_b = 0.6, and then it increases as the shoreline is approached.

For a constant relative depth there are some differences in the surf-wave height to depth ratio from study to study (Table I). For example, H/h varies from 0.44 (Horikawa and Kuo) to 0.62 (Nakamura) for h/h_b = 0.6. Since the original data contained significant scatter, these differences are expected. This discrepancy could also be partly due to the use of different initial wave steepness by the three investigators. The measurements of Nakamura et al. show that the surf-wave height ratio H/H_b decays more rapidly with depth for initially steeper waves. However, since all of the experimental surf-wave height-to-depth ratios, H/h, are less than 0.80, the hypothesis that the surf-waves have transformed from initially spilling solitary breakers to breaking long waves, or surf-bores, is not disproved. In fact, this hypothesis is also supported by previous field work of Huntley and Bowen (1975a) and the measurements herein (see Discussion of Results).

Galvin (1968) experimentally demonstrated that breaker type (eg., spilling, plunging, collapsing, and surging) is primarily a function of beach slope and secondarily a function of the deep water wave steepness. For beach slopes of 0.05, 0.10, and 0.20, Galvin (1969)

found that the distance over which the wave changed from a plunging breaker to a surf-bore could be divided into two characteristic distances. The 'plunge' distance is the horizontal distance between the point where the crest first becomes vertical and the point where the crest makes contact with (or plunges onto) the beach slope. The 'splash' distance is the distance between the point where the crest first contacts the beach slope and the point where the splash from the rebounding crest lands. Shoreward of this splash point Galvin observed that the wave continues as a surf-bore to the run-up limit. Similar experiments for spilling breakers have not been performed.

Surges, or progressive long waves, have been classified into three types (Sandover and Zienkiewicz, 1957): (1) undular surges, (2) undular-with-breaking surges, and (3) steep fronted breaking surges (Figure 12). Favre (1936) experimentally determined that the transition from undular surge to breaking undular surge occurs at $h_1/h_2 = 1.34$. Sandover and Zienkiewicz (1957) measured h_1max, the depth of the first undular crest, and h_1min, the depth of the first undular trough (Figure 12); the undular surge to breaking undular surge transition was characterized by $h_1max/h_2 = 1.59$ and $h_1min/h_2=1.1$. Defining an average crest depth as $\bar{h}_1 = 1/2(h_1max + h_1min)$, we find that $\bar{h}_1/h_2 = 1.34$, a value in agreement with the transition value found by Favre. No experiments measured h_1/h_2 for the transition from a breaking undular surge to a fully breaking surge. However, studies of the analogous types of hydraulic jumps (defined as a stationary surge in which the stream speed is equal and opposite to the surge wave velocity) in horizontal channels yield approximate

values for h_1/h_2.

Binnie and Orkney's (1955) measurements show $h_1/h_2 = 1.35$ for the transition from an undular hydraulic jump to a breaking undular hydraulic jump, and $h_1/h_2 = 1.75$ for the transition from a breaking undular jump to a fully breaking jump. Bakhmeteff and Matzke (1936) observed the transition from a breaking undular jump to a fully breaking jump occurs when $h_1/h_2 \simeq 2.0$. Chow (1959) and Henderson (1966), in summarizing past hydraulic jump experiments, report the transition between jump types in terms of the Froude number F_2 where $F_2 = v_2/(gh_2)^{1/2}$ and v_2 is the stream velocity prior to the jump (for a progressive surf-bore, v_2 is the negative of the surf-bore celerity when viewed from a coordinate system moving with the bore crest). They found undular jumps are dominant for $F_2 < 1.7$ ($h_1/h_2 < 1.96$) and fully breaking jumps are the rule when $F_2 > 1.7$. The ratio h_1/h_2 is a calculated value using the equation

$$h_1/h_2 = 1/2[(1 + 8 F_2^2)^{1/2} - 1] \qquad (19)$$

This relationship was derived from the momentum equation for the hydraulic jump in steady, frictionless, uniform flow in a horizontal channel (Henderson, 1966). Equation (19) is known to be in good agreement with hydraulic jump data. Henderson (1966) does note that the breaking undular jump can occur for $1.35 \leq h_1/h_2 \leq 1.75$ but that exact values are dependent on bed roughness.

This surge and hydraulic jump data may be summarized by noting that $h_1/h_2 = 1.35$ denotes the transition from undular to breaking undular type for both surges and hydraulic jumps. For $h_1/h_2 = 1.75$ to

2.0 the hydraulic jump type changes from breaking undular to fully breaking. Because of the identical values for the undular to breaking undular type, the value $h_1/h_2 = 1.75$ may also be used with confidence for the breaking undular surge to fully breaking surge transition.

Extensive field measurements (Huntley and Bowen, 1975a) of current velocities in surf zones on a gently sloping beach (s = 0.014) show that: (1) many waves traverse the surf zone simultaneously, (2) breakers transform from spilling solitary type waves to saw-toothed shaped, bore-like surges, and (3) undular surf-bores occur near the shoreward edge of the surf zone. Spectra from these measurements revealed a feature common to both steep (s = 0.13) and shallow (s = 0.01) beaches; the spectral energy density decays exponentially with increasing frequency, suggesting the form

$$S(f) = S_i \exp(-pf), \quad f_i > f > 1.0 \text{ sec}^{-1}. \qquad (20)$$

where S_i is the energy density at the predominant incident wave frequency $f = f_i$. Since a similar decay was found in our measurements, further discussion is presented later in the Results section.

Gallagher (1972) presented photographs of breaking and non-breaking undular surf-bores in a Hawaiian ocean surf zone. The bottom topography in this case is not common to all nearshore regions; the waves encounter a relatively steep slope at the outer edge of the reef before traveling across a flat rough reef. Once the waves are over the flat reef, the breaking process decreases in intensity and small waves begin appearing behind the wave crest. He reported approximate Ursell numbers ranging from 300 to 800 but did not discuss h_1/h_2 values.

Simultaneous measurements of the local onshore-offshore orbital velocity and the bottom pressure led Steer (1972) to conclude that most of the motion within a Pacific Ocean surf zone (s = 0.04) is wave induced. A coherence of 0.9 between the onshore-offshore orbital velocity and the pressure measurements supported this contention. Suhayda and Pettigrew (1974) measured the celerity of breaking and nonbreaking waves on an Atlantic Ocean beach and concluded that the average wave celerity for breaking waves agreed generally with the finite amplitude long wave theory of Keulegan and Patterson (1940). Their data also showed considerable scatter and a systematic disagreement with theory for points near the shoreline. They suggested that surf-bore shape and interaction with low frequency backwash may be significant factors influencing the celerity of surf-waves. Schiffman (1965) observed a transition zone between the surf and swash zones in which the return flow of swash collides with the incoming surf-bores. This resulted in a highly turbulent flow, a broad velocity energy spectrum and a bimodal sand size distribution.

Low Frequency Motion in the Surf and Swash Zones

Field observations in the swash zone reveal that the time interval between successive swashes is longer than the predominant incident wave period, increasing as the beach slope decreases (Emery and Gale, 1951; Huntley and Bowen, 1975a). Emery and Gale (1951) attributed this longer period to both complete breaker decay prior to reaching the swash zone and swash-backwash interaction. They observed that some small breakers or bores decayed completely or were destroyed by

overtaking larger bores. They concluded that swash interaction was especially important on gently sloping beaches and described the following event. After a large swash has traveled up the slope, its substantial volume of water takes a relatively long time to accelerate seaward as a backwash. The backwash of this large swash is then able to destroy several successive small swashes. For a beach slope of $s = 0.03$, measured swash periods were approximately 25 to 30 seconds.

Waddell (1973) demonstrated that for beach slopes steeper than $s = 0.10$, the duration of an uninterrupted swash was dependent on the incident bore height at the shoreline and not on the input wave period. This bore height dependence can cause the uninterrupted swash period to differ from the input wave period. If the uninterrupted swash period exceeds the incident wave period, then interaction between successive swashes occurs because the following wave enters the swash zone before the preceding swash has left as backwash. This results in the swash-backwash interaction suggested by Emery and Gale (1951).

Low frequency swash may also be caused by standing or progressive edge waves (waves trapped against the beach by refraction). Observations of edge waves with a period twice that of the incoming waves have been measured by Huntley and Bowen (1975a; 1975b) who noted that strong interactions took place between successive breakers such that an alternating sequence of surging and collapsing breakers occurred ($s = 0.13$). A breaker, interacting with the strong backwash of the previous wave, would collapse on the lower beach slope with low swash. Before the backwash could begin the following wave would travel far up the beach through the standing water as a surging breaker. This would

lead to a strong backwash which then interacts with the third breaker causing it to collapse on the lower slope with low swash. This process would then be repeated.

Additional observations of swash on a steep beach (s = 0.13) indicate that standing waves can occur due to reflection of incident long period, nonbreaking swell of low steepness (Syhayda, 1974). The standing wave then has the same period as the incoming long period swell.

On steep beaches (s = 0.10) subharmonic edge waves and reflected long period swell are the major types of low frequency wave motion most often observed. On shallow beaches (s = 0.01) complete decay of small breakers, large bores overtaking small bores, and swash-backwash interactions have all been suggested as mechanisms causing low frequency swash.

EQUIPMENT AND PROCEDURES

This section describes the equipment and procedures used to measure the spilling breaker-to-surf bore transformation. A wave-surf bore classification is developed with the aid of time-lapse photographs, and water surface elevation measurements allow the determination of the depth at the wave crest, h_1, the lowest depth at the trough preceding the crest, h_2, and the wave period T. These variables are then used to determine if the wave and bore types can be quantitatively characterized.

Equipment

Three instruments were utilized simultaneously to measure wave parameters within surf zones: (1) resistance wire wave staff for determining the local water surface time history, (2) a super-eight time-lapse color photography camera to record wave and bore types, and (3) an electromagnetic current meter to measure the onshore-offshore flow.

The wave staffs are constructed of nichrome wire wound on 2.54 cm diameter threaded pvc plastic pipe three meters in length. The threading allows for a higher resistance per unit staff length (1.64 ohms/cm). A two kilohertz, ten volt peak-to-peak signal is provided to the wave staff channels with a maximum of six staffs able to operate from the same signal source. This voltage signal is then converted to a proportional current which is used to drive the wave staff probe. Because of this conversion, current in the probe will not vary with a change in probe resistance. And voltage across the probe will be directly proportional to probe resistance and thus to the length of staff not immersed in salt water. The current wave form is sinusoidal with a maximum output of four milliamperes peak-to-peak. This provides two volts peak-to-peak across the wave staff probe; this voltage is then rectified and peak detected to provide a one volt maximum output signal. A static calibration of the staff in seawater is shown in Figure 13. This calibration is accomplished by successively lowering the probe into the water in increments allowing equilibrium to occur at each length of immersion.

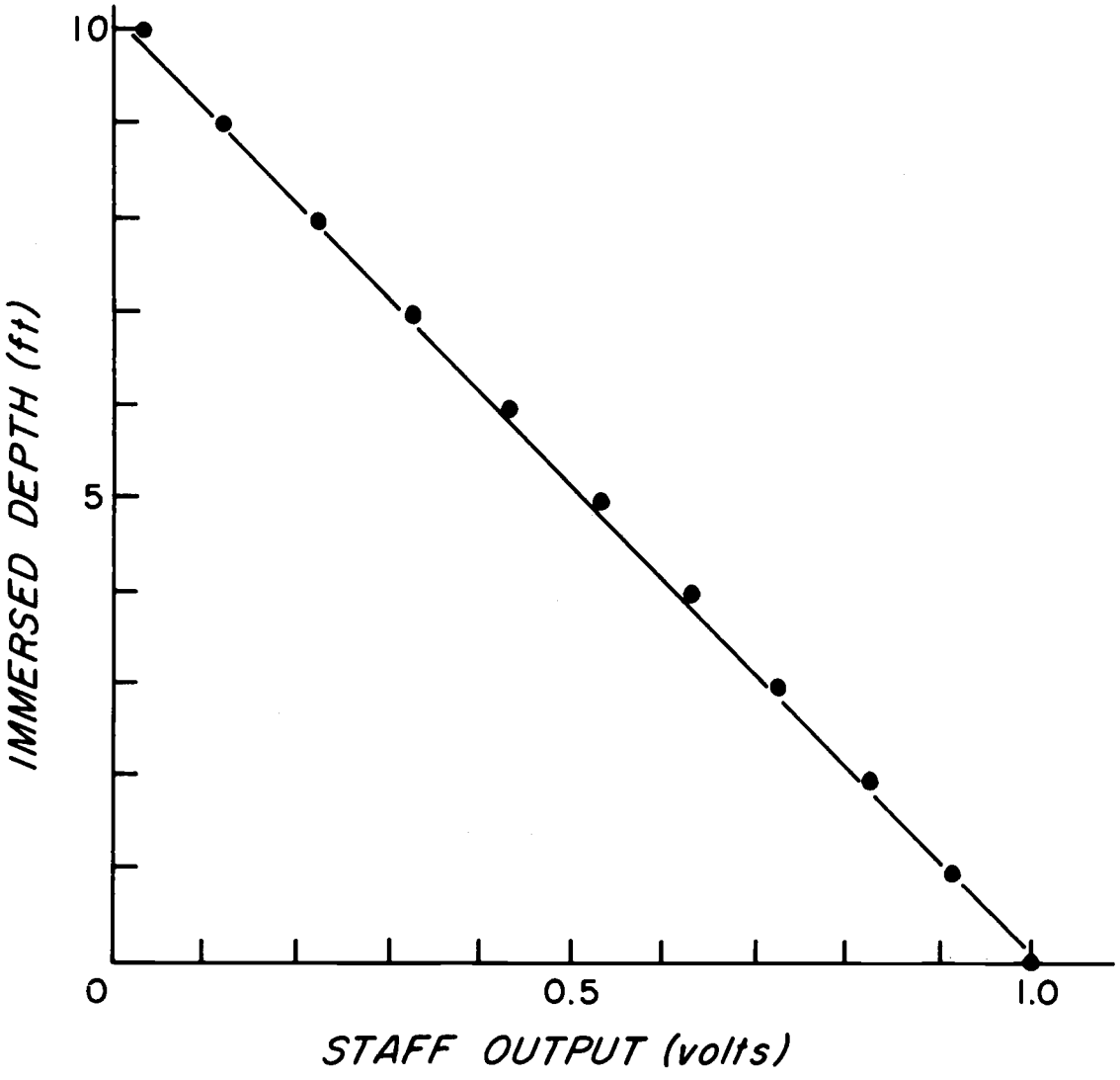

Figure 13. Static calibration of wave staff.

An accurate dynamic calibration of the wave staff could not be performed due to a lack of facilities. However, a qualitative check of the instrument's response was made by oscillating the probe in salt water. For approximate amplitudes of 30.0 and 60.0 cm and periods of one-half and one second, respectively, the response appears adequate during both immersion and withdrawal of the probe.

A super-eight millimeter Nizo motion picture camera with an eighty to two hundred millimeter zoom lens was used to record the wave and breaker types. The time lapse mode of operation was used with a time interval of one photo per second. An elevated site on the beach was chosen for camera placement.

Onshore-offshore currents were measured with a Marsh-McBirney Model 711 electromagnetic current meter, mounted 21.0 cm above the sea-bed. The probe is 2.54 cm in diameter and 26.7 cm long with four electrodes mounted at ninety degree angles to each other around the probe's circumference. The electrodes function in pairs to detect the electric field created by the movement of water through the probe's magnetic field. Two components of the water velocity perpendicular to the probe axis are thus measured. A review of the method of operation and accuracy of electromagnetic current meters may be found in Stolzenbach and Howerton (1975).

Static calibration of the Marsh-McBirney Model 711 current meter is accomplished in a towing facility where the flow is known to within plus or minus two percent. The output signals from the probe may deviate from exactly linear response to increasing water flow due to minor variations in flow streamlines at increasing velocity. This

factor is small enough to guarantee that the outputs are within two percent of nominal over the range of the instrument (Marsh-McBirney, 1972).

Field Procedures

The wave staff probe is attached to a 3.8 cm diameter aluminum rod which is firmly anchored to the beach with three guy wires secured to metal stakes driven into the beach face. In addition, the lower end of the support rod is cemented into a one gallon can that is buried one meter below the sand surface. The wave staff is attached to this support rod on the shoreward side to block the staff from run-up caused by rapid horizontal currents or by impacts of bore fronts.

Two support mountings and two wave staffs are placed within the surf zone during low-low tide. Staff separation distances are listed in Table II. The wave staffs are calibrated one volt per 3.05 meters of nonimmersed staff each time they are used. The output voltages from the wave staffs are recorded on a high frequency response Gould-Brush Model 440 analog three channel chart recorder (1-80 mm and 2-40 mm wide channels) at a rate of five mm per second). Both the wave staff electronics and the Brush recorder are powered by a heavy duty twelve volt battery through a Powercon Model 12ESW25 dc-to-ac converter. Over the usual twenty minute recording time no significant power drain on the battery would take place.

After the wave staffs are mounted in the surf zone a beach profile is surveyed with a self leveling telescope and a graduated staff. When the tide is sufficiently high to provide a minimum depth of at least

TABLE II. Wave and Surf Parameters

Run Ident.- Location	Staff Separation m.	Mean Depth, $\bar{h}$ cm.	$H_{1/3}$, $T_{1/3}$* deep water cm.	sec.
9/2 I Sea	23.8	75.0	61.0	10.0
9/2 I Shore		57.2	61.0	10.0
9/2 II Sea	23.8	108.7	61.0	10.0
9/2 II Shore		96.1	61.0	10.0
9/16 Sea	38.4	108.2	61.0	10.0
9/16 Shore		63.8	61.0	10.0
8/14 I Sea	9.5	36.3	61.0	8.0
8/14 I Shore		22.3	61.0	8.0
8/14 II Sea	9.5	33.6	61.0	8.0
8/14 II Shore		20.2	61.0	8.0
8/18 I Staff		60.4	30.5	8.0
8/18 I C.M.**		60.4	30.5	8.0
8/18 II Staff		85.0	30.5	8.0
8/18 II C.M.		85.0	30.5	8.0

* Data from Marine Science Center, Newport, Oregon

** C.M. = Current Meter, 21.0 cm. above bottom.

Beach slope s = 0.0067

a half a meter at both staff positions, measurements are begun. A second run was usually performed before the tide was maximum.

Field Site

Simultaneous field measurements of surf wave parameters have been obtained in an ocean surf zone typical of broad, low, sandy beaches on the west coast of the United States. The measuring site is located at Agate Beach, Oregon, five kilometers north of the city of Newport (Figure 14A). The tide has a diurnal inequality with a maximum diurnal range of approximately three meters during the measuring periods. The sediment is a fine grained (median diameter 194 microns) quartz-feldspar sand, and the surf zone profile has an uniform slope of 0.007 (Figure 14B). This location was chosen because of several advantageous field characteristics. During the months of August and September most of the waves impinging on the beach are generated by north to northwest winds circulating about the high pressure cell located off the Oregon coast. At this site the waves refract so that near the beach their crests are approximating parallel to the shoreline. This results in a minimal longshore current. In addition, Yaquina Head just to the north of Agate Beach blocks the surf zone from the direct force of the prevailing winds.

Measuring Difficulties

Obtaining accurate and meaningful measurements of the water surface elevation within the surf zone is a difficult task. Meaningful measurements must account for or eliminate (1) double valued surface

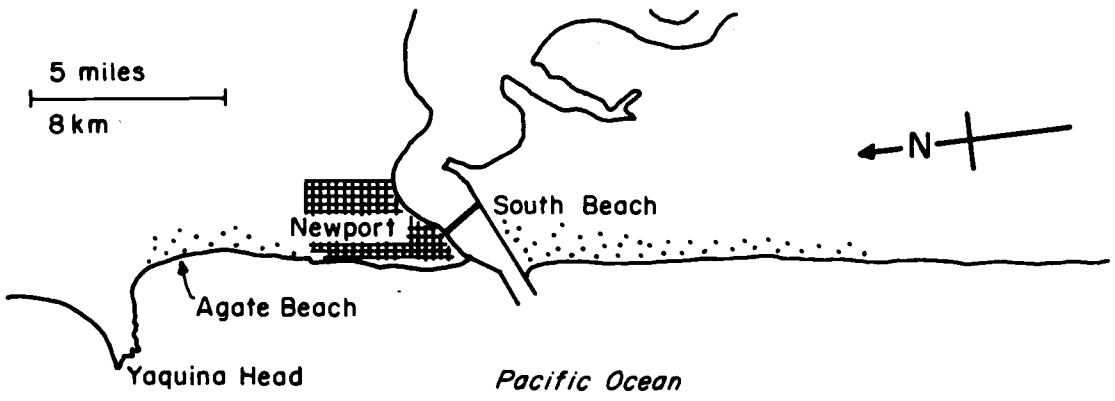

Figure 14A. Location of field site at Agate Beach, Oregon.

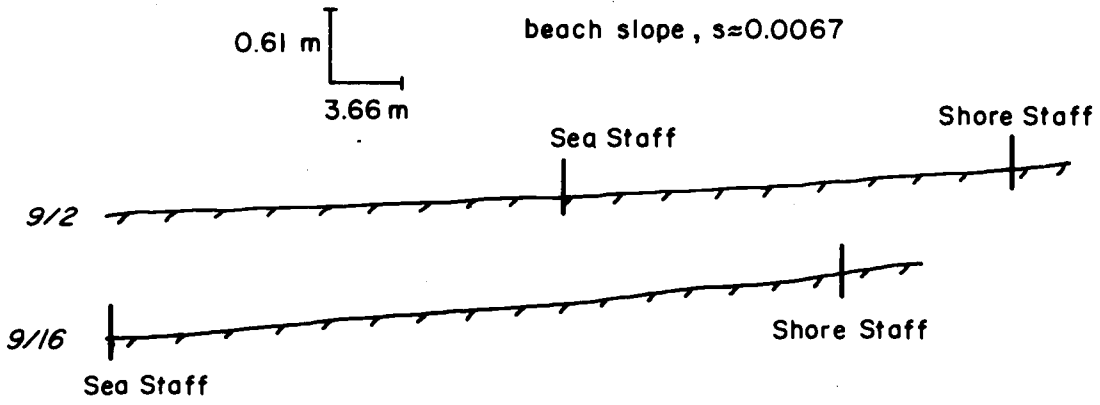

Figure 14B. Beach slope profiles in surf zone, Agate Beach, Oregon.

elevation caused by the crest curling onto the shoreward wave face, (2) surface elevations with air-entrained water, and (3) run-up on the staff.

Double valued surface elevations occur whenever waves break by plunging, whether in the main breaker zone or smaller waves breaking within the surf zone. Since the staffs were positioned inshore of the main breaking zone, this case represents a small proportion of the total number of waves passing the probe as verified with the time-lapse photographs.

The air-entrainment process is one of the primary characteristics of waves within surf zones. During the initial breaking sequence most of the waves transform into asymmetrical wave profiles with air entrained on the steep shoreward face (Figure 15). Figure 16 depicts a typical analog recording of the voltage output from the wave staff. As the breaking bore front passes a smooth trace is obtained in spite of the irregular surface of air-entrained water. This measured depth is probably less than the highest level of the air-with-water globs and slightly greater than the air-entrained water below. Although this type of measurement does not record the bore face in detail, it is representative of the saw-toothed asymmetry of both the wave profile and the onshore-offshore current velocity. This was verified by the photographs and current measurements.

The largest error associated with the wave staff probes is due to run-up caused either by breaker impact or large horizontal current speeds. Except for two extreme cases, high speed photography (64 frames/second) showed that the mounting system sufficed in reducing

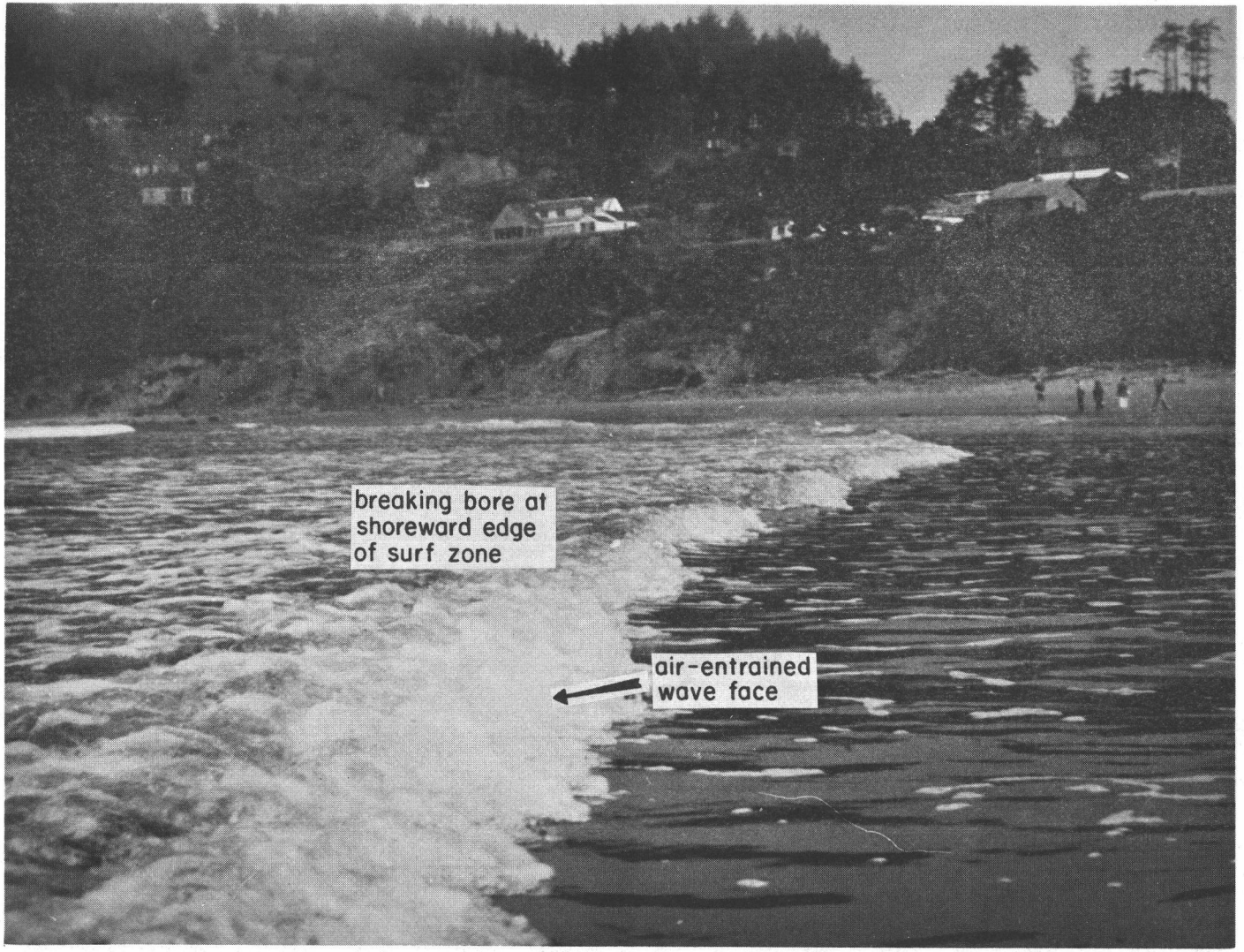

Figure 15. Breaking surf-bore near shoreward edge of surf zone.

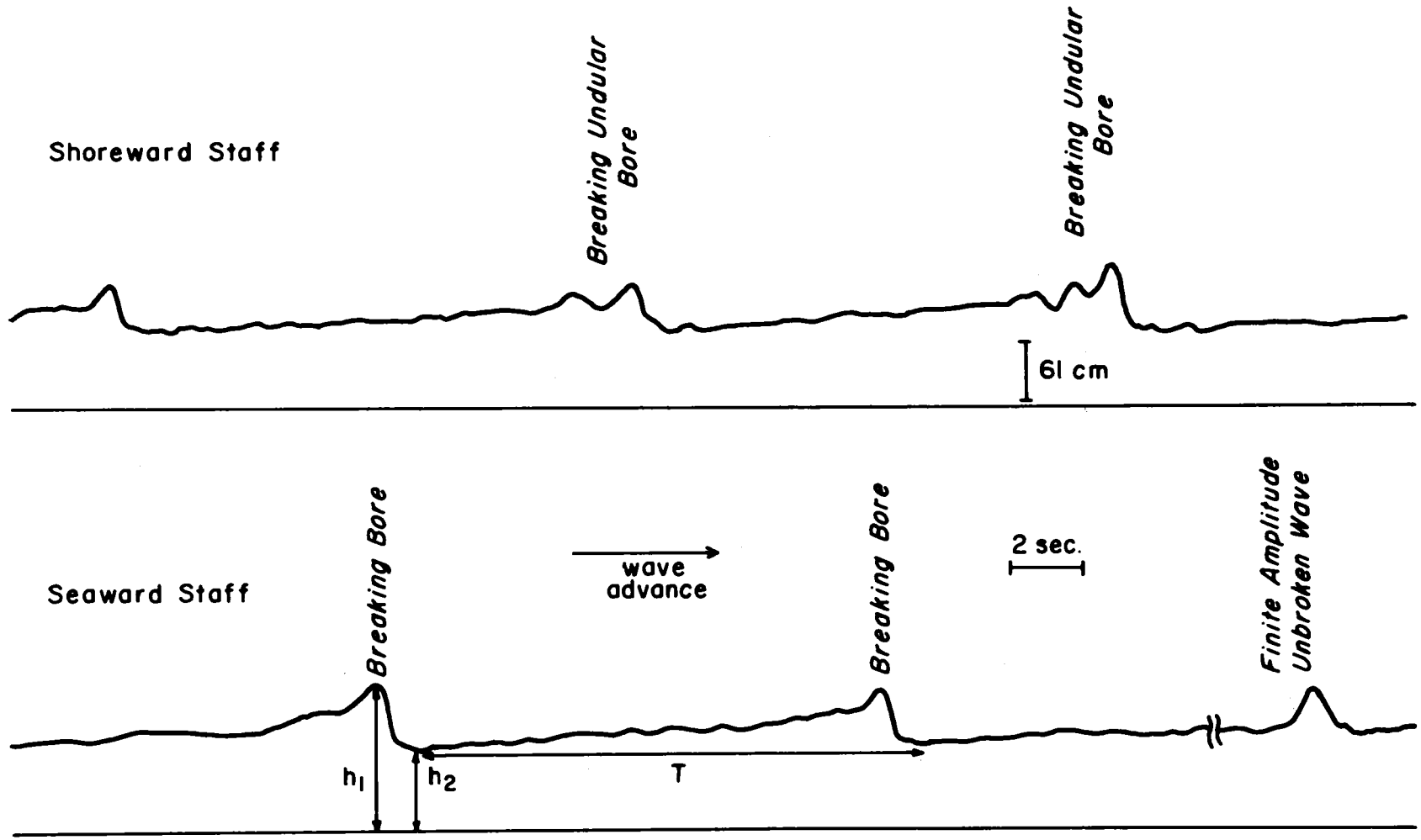

Figure 16. Characteristic analog trace of voltage output from wave staff, including definitions of h_1, h_2, H and T.

this error to acceptable limits. One case occurs when the waves break by plunging and form very strong bores, the bore height being many times the mean water depth. These strong bores were observed during low tide. The second extreme case is the breaking of large waves directly on the staff. As stated previously, measurements were not taken during low tide nor near the initial breaking position of the dominant waves.

Data Treatment

The field measurements are designed to provide information on waves and breakers within the surf zone. The wave data are treated in steps in order to successively obtain more detailed information on wave characteristics within surf zones. First, the surface elevation time histories are compared to the time-lapse photographs, and the wave crests on the analog record are identified according to wave and bore type. This is done for the data taken synchronously at two surf zone locations so that the wave transformations between the two positions for each identifiable crest are obtained. Then the analog surface elevation record is used to measure the two shallow water depth parameters, the depth of the water, h_2, at the trough preceding the wave crest, and the maximum depth, h_1, at the wave crest. These two parameters are defined in Figure 16. The wave or bore height H is then $h_1 - h_2$.

The analog chart records of the surface elevation and current are next digitized for spectral analysis. The digital process requires the following procedures: (1) each record is digitized in fifty cm

sections, the maximum length possible on the available equipment. The time axis is incremented in 0.02 inch (0.10 seconds) lengths and the surface elevation trace is measured to the nearest 0.01 inch. (2) The fifty cm sections are then matched together to provide a continuous digital record of the time series. The method used to accomplish this matching was to overlap the digitization of the end of each section into the beginning of the next section by about 1.5 cm. (3) Once the overlap is identified by comparing the two records it is removed from the digital record. (4) Plots of the digital record are then made to test its resemblance to the original record. If the digital and analog traces are nearly identical then the digital record is ready for analysis.

DISCUSSION OF RESULTS

Field measurements were obtained at Agate Beach on four days during August and September, 1974; the major portion of the data consists of synoptic measurements of the surface elevation at two surf zone positions located along an offshore line. Table II shows the staff separation distances and other relevant data. Simultaneous measurements were also obtained of the surface elevation and the on-shore-offshore current. The incident wave conditions were approximately the same during the observations; the significant deep water wave height and period (Table II) were derived from seismometer measurements from the O.S.U. Marine Science Center in nearby Newport, Oregon (Bodvarsson, 1975; Enfield, 1974).

This section is divided into two parts. Part one describes

component breaking waves and surf-bores with the aid of the time-lapse photographs and the analog chart records of the local surface elevation. The depth ratio h_1/h_2 and the Ursell number HL^2/h^3 are calculated and discussed in relation to the wave types. In part two, dimensional and non-dimensional spectra of the surface elevation and current are analyzed for the frequency content higher than the dominant incident waves.

Component Waves and Surf-bores in the Surf Zone

An advantage of studying waves in shallow water is that each wave travels with approximately the group velocity, so that each wave may be identified as a packet of energy. In addition, the waves are frequently separate, isolated crests. For these reasons identifying component waves and their transformations is a simple and physically meaningful method of analysis for waves in shallow water.

The most frequently measured surf wave type is the breaking surf-bore. Figure 17 is a photograph of a newly formed breaking surf-bore just shoreward of the breaker zone, and Figure 15 is a photograph of the breaking surf-bore near the swash zone edge of the surf zone. These photographs show the distinctive steepening of the shoreward wave face as the bore travels shoreward. The major characteristic of the recorded surface elevation is the extreme saw-toothed asymmetry about the vertical crest (Figure 16, page 53). This is caused by the contrast between the steep breaking shoreward surface slope and the low seaward surface slope.

A similar but less frequently measured surf wave is the breaking

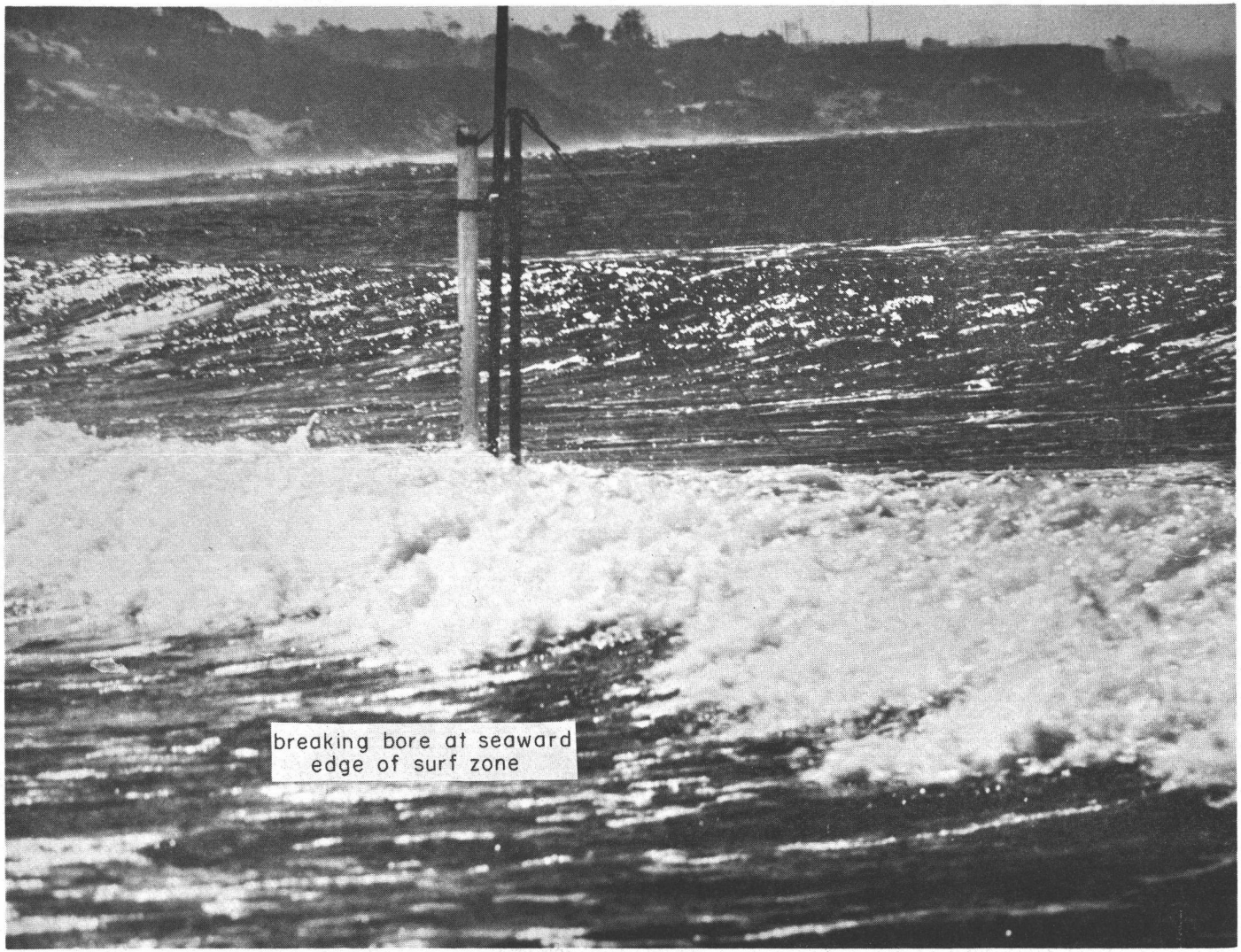

Figure 17. Breaking bore at seaward edge of surf zone.

undular surf-bore. The small waves, or undulations, just seaward of the crest are easily identified on the analog trace of the surface elevation (Figure 16). Its occurrence on a gently sloping sand beach has been reported previously on only one occasion (Huntley and Bowen, 1975a). Figure 18 is a photograph of the breaking undular surf-bore near the shoreward edge of the surf zone where the single small wave formed at the crest has separated slightly from the bore crest.

Another surf wave type is the incipient breaking wave. Incipient breakers are, of course, typical of the breaker zone (see part one of this thesis), but some occur in the surf zone as well when incident waves of low steepness do not break in the main breaker zone. This overlapping of the nearshore regions is unavoidable in the field due to the wide spectrum of waves, but on these occasions the incipient breakers within the surf zone were a small percentage of the total number of observed waves.

In addition to waves that are breaking or have already broken, non-breaking waves were measured in the surf zone. Most of the non-breaking waves have medium to large amplitudes, and their local surface profiles show symmetry about a vertical line through the crest (Figure 16).

Table III shows the mean and standard deviation for h_1/h_2 for 844 surf-bore observations from eight different records, and Figure 19A is a histogram, or frequency distribution, of these h_1/h_2 values. These histograms are significant descriptions of the surf-bores and non-breaking wave types. The histogram of h_1/h_2 for the surf-bores is narrow with most of the h_1/h_2 values being in the range 1.5 to 1.7.

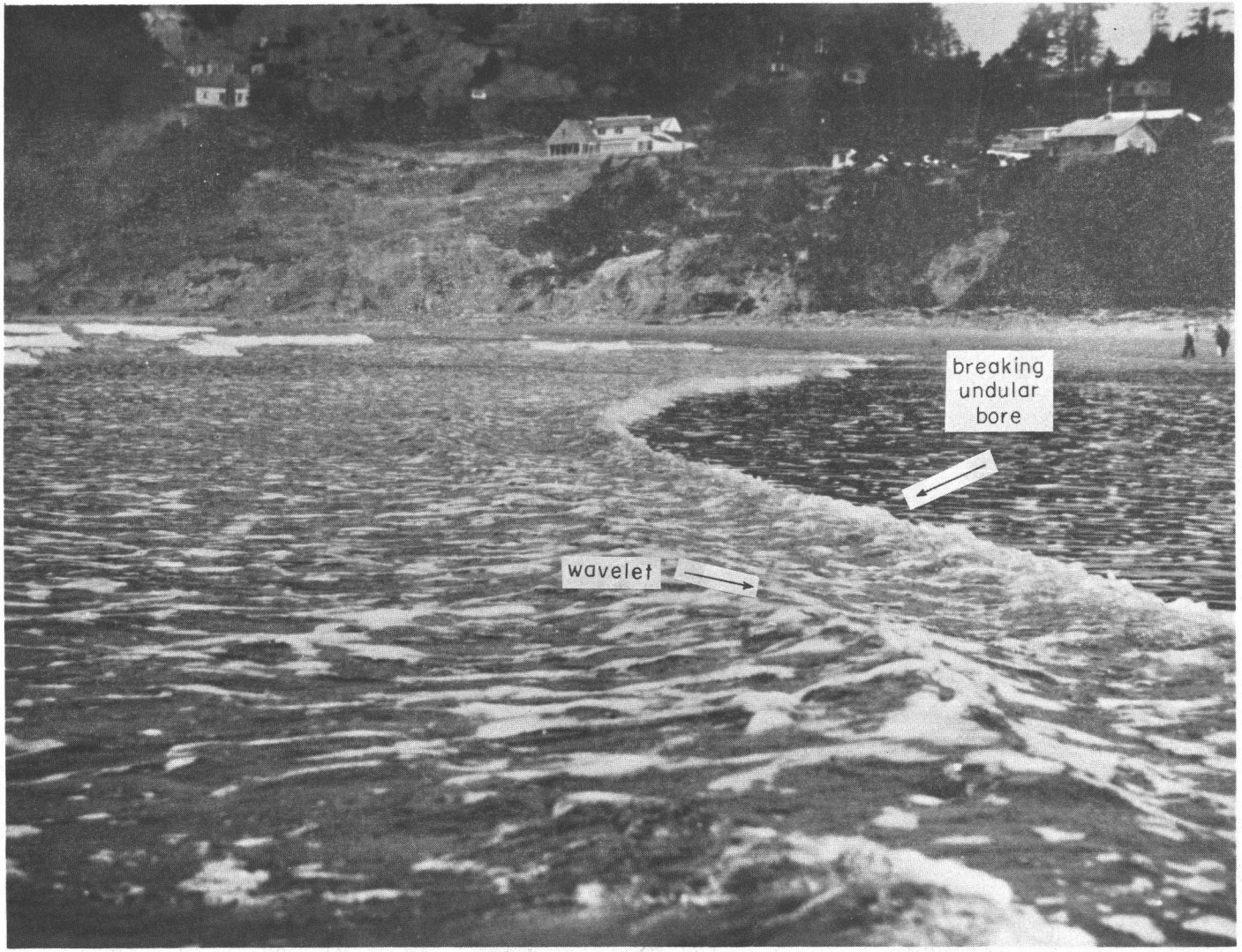

Figure 18. Breaking undular bore with single wavelet near shoreward edge of surf zone.

TABLE III. Mean and Standard Deviations of the Dimensionless Parameters h_1/h_2 and the Ursell Number $U_r = (h_2-h_1)T^2/ h_1^2$.

1. Surf-bores

Station	h_1/h_2	S.D.	N	U_r	S.D.	N	T sec	S.D.	N	$\bar{h}$ cm
9/2 I Sea	1.60	0.16	70	1052	780	67	10.0	3.5	66	75.
9/2 I Shr	1.61	0.20	38	1419	1300	31	9.1	4.5	33	57.
9/2 II Sea	1.61	0.08	84	714	364	83	10.1	2.7	81	109.
9/2 II Shr	1.63	0.15	65	752	557	59	9.2	3.7	59	96.
9/16 Sea	1.70	0.17	16	655	455	15	8.7	3.0	15	108.
9/16 Shr	1.65	0.14	84	670	479	70	6.9	2.3	70	64.
8/18 I	1.65	0.20	60	846	855	69	6.8	2.7	56	60.4
8/18 II	1.72	0.16	38	442	297	42	6.0	2.0	36	85.

2. Non-breaking Waves

9/2 I Sea	1.23	0.13	18	126	209	16	3.7	2.1	16
9/2 I Shr	1.24	0.18	26	162	292	21	3.4	2.4	19
9/2 II Sea	1.29	0.15	27	44	37	21	3.3	1.0	21
9/2 II Shr	1.33	0.20	40	87	70	20	4.2	2.2	21
9/16 Sea	1.44	0.23	72	394	351	57	7.7	2.4	62
9/16 Shr	1.37	0.21	32	202	244	22	4.5	1.8	24
8/18 I	1.35	0.18	83	197	253	44	4.5	1.9	44
8/18 II	1.33	0.19	91	168	171	40	5.0	1.7	40

S.D. = Standard Deviation

N = Number in Sample

$\bar{h}$ = Mean Depth

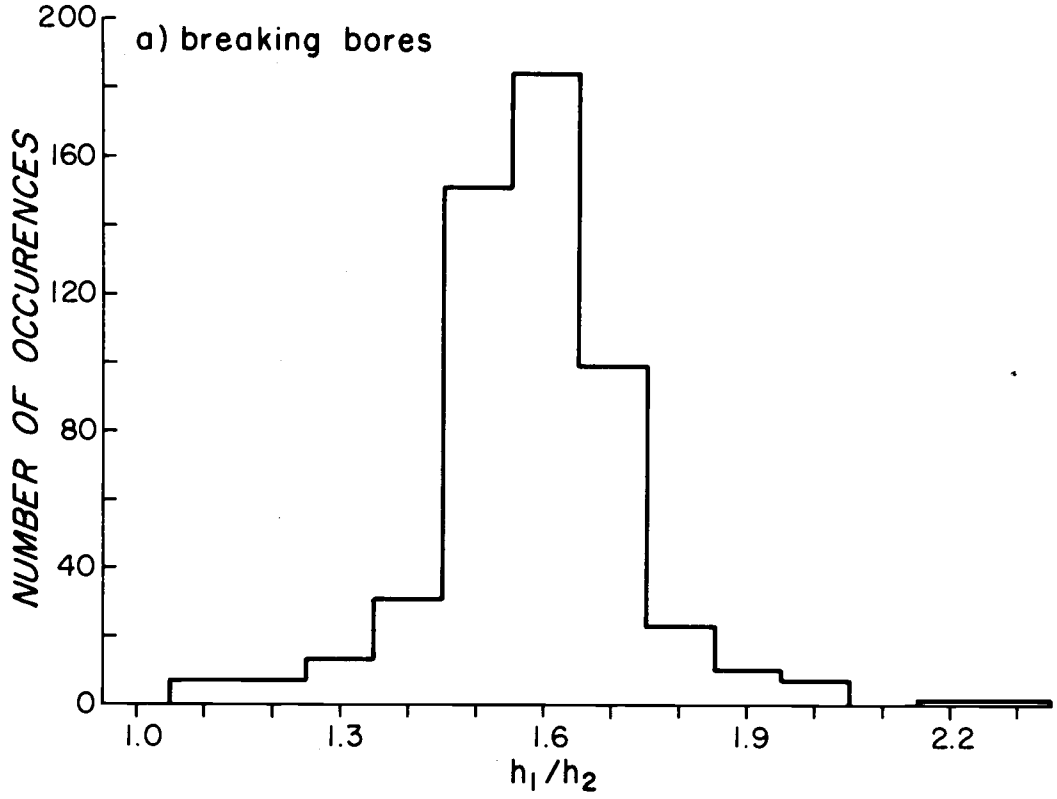

Figure 19A. Histogram of h_1/h_2 for all surf-bore data.

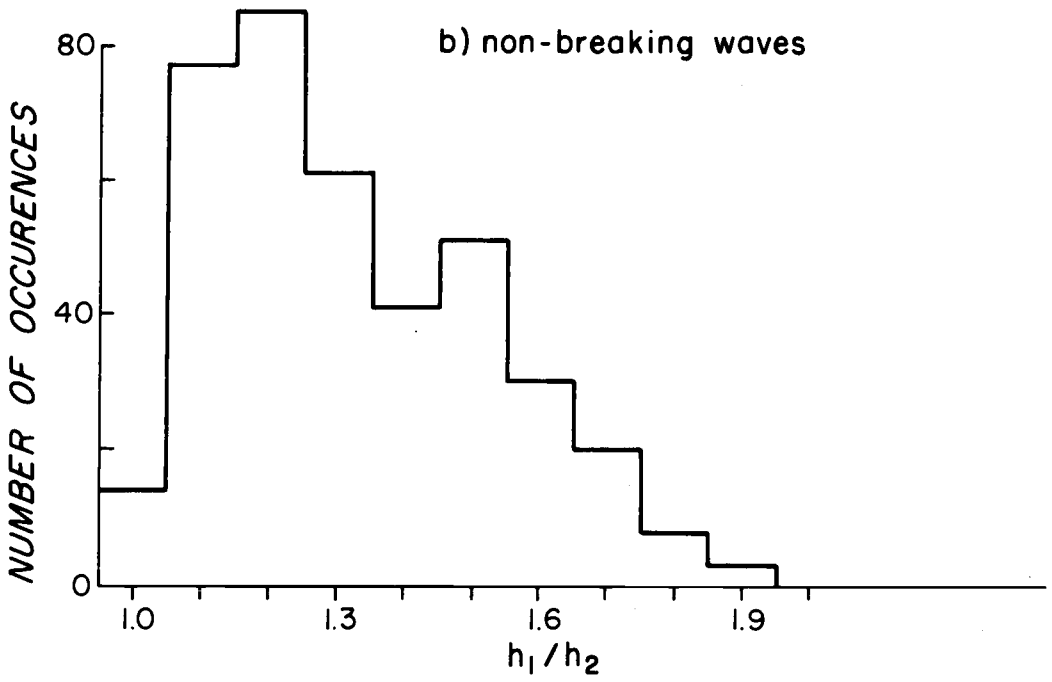

Figure 19B. Histogram of h_1/h_2 for all non-breaking wave data.

This suggests that most of the surf-bores are undergoing a similar type of transformation. The histogram of h_1/h_2 for the non-breaking waves is a wider distribution with many low amplitude waves and some near breaking waves; the non-breaking waves encompass the entire range of prebreaking wave stages.

The mean h_1/h_2 value (1.64) for the surf-bores differs little from the mean value for each individual record (Table III). Hence, it is a representative value for surf-bores. This value is lower than the theoretical value (1.8) for maximum height solitary waves; a value that is often applied in studies of breakers in surf zones. In terms of H/h, the average measured value is 0.64, and H/h = 0.8 for the solitary wave of maximum height. As evidenced by the histograms (Figure 19A) most of the waves continue breaking even though this depth ratio is lower than 0.80. One explanation for this is the amplitude dispersion mechanism (see Theory) which causes the continual steepening of the shoreward wave face. Amplitude dispersion is characteristic of the finite amplitude long wave equations.

The surf bore data are separated into surf-bores and undular surf-bores in Table IV; unfortunately, the mean h_1/h_2 values are not significantly different. For the undular surf-bores, the h_1/h_2 values are all within the empirically determined transition values ($1.34 \leq h_1/h_2 \leq 1.75$) delimiting breaking undular surges (see Previous Observations). The surf-bore values are lower than the transition value (1.75) between breaking undular surges and fully breaking surges.

Undular surf-bores were observed on five of the eight records; on these days the undular surf-bores occur more frequently at the

TABLE IV. Mean and Standard Deviation of the Dimensionless Parameters h_1/h_2 and U_r for surf-bores and undular surf-bores.

1. Surf-bores

Station	h_1/h_2	S.D.	N	U_r	S.D.	N
9/2 I Sea	1.60	0.16	70	1052	779	67
9/2 I Shr	1.61	0.21	38	1419	1320	31
9/2 II Sea	1.61	0.08	84	714	363	83
9/2 II Shr	1.63	0.15	65	752	557	59
9/16 Sea	1.70	0.17	15	655	455	15
9/16 Shr	1.65	0.14	84	670	479	70
8/18 I	1.65	0.20	60	846	855	69
8/18 II	1.69	0.40	38	442	297	42

2. Undular Surf-bores

9/2 I Sea	1.55	0.12	21	985	438	20
9/2 I Shr	1.59	0.12	38	1700	1439	32
9/2 II Shr	1.56	0.11	24	757	402	23
8/18 I	1.66	0.05	11	1174	493	10
8/18 II	1.72	0.24	6	694	351	6

shoreward wave staff. However, there is no consistent pattern between the number of undular surf-bores observed and the absolute depth when the values from different records are compared.

The depth ratio h_1/h_2 was also calculated for the incipient breakers; however, these values are likely to contain an unknown error due to significant run-up on the measuring staff. For the incipient breakers, the mean h_1/h_2 value equals 1.8 with a standard deviation of 0.2. Such a mean value, if accurate, supports the hypothesis that many of the waves are initially spilling solitary breakers. It is possible that the h_1/h_2 values in excess of 1.8 are due to splash-up associated with breakers that partly plunge. Lower h_1/h_2 values may be due to measuring errors in that the wave did not break directly on the staff; these values may also be due to the breaking of long waves rather than solitary-type waves.

These surf-bore and non-breaking wave measurements support the observations of Huntley and Bowen (1975a) for waves on gently sloping beaches in that (1) incipient breakers resemble spilling solitary waves and (2) spilling breakers transform into saw-toothed shaped long waves, or surf-bores. First, the surf-bore h_1/h_2 mean values are lower than the theoretical breaking criterion for solitary waves, but they are not considerably lower. If they were much lower, it would likely be that many of the incipient breakers are breaking long waves rather than spilling solitary breakers. The h_1/h_2 values for the measured incipient breakers bear this out even though they are subject to some doubt due to measuring errors.

This indicates that the incipient breakers spill with h_1/h_2 on the

order of 1.8; as they travel shoreward they transform to long waves has lower h_1/h_2 values. This transformation explains why the waves continue to break even at low h_1/h_2 values. The measured non-breaking waves support this composite picture of the breaker and surf zones due to their solitary wave characteristics: (1) the local surface profile is symmetric about a vertical line through the crest rather than the saw-toothed bore shape, and (2) the mean h_1/h_2 values are less than the solitary breaking index, but many are large enough to be breaking due to amplitude dispersion if the waves were also long enough.

Following Ursell's (1952) suggestion that the Ursell number may indicate the applicable wave theory, U_r was calculated for waves within the surf zone. Longer period waves should be more bore-like at a given surf zone position since they have most likely broken further seaward. U_r is calculated according to the equation

$$U_r = H L^2 / h^3 \qquad (21)$$

Utilizing $H = h_1 - h_2$, $h = h_2$, $L = T(gh_2)^{1/2}$ where T is an approximate wave period or decay time, equation (21) becomes

$$U_r = g(h_1 - h_2)T^2 / h_2^2 \qquad (22)$$

Here T is defined as the time between the initial arrival of a wave crest and the subsequent decay of the local surface elevation to the same depth h_2 as at the time just prior to the crest arrival (Figure 16).

Table III contains the mean U_r values for 663 identifiable and isolated wave crests. U_r ranged from 442 to 1419 for the breaking

surf-bores and from 44 to 394 for the non-breaking waves. This large difference in the mean U_r values for surf-bores and non-breaking waves is evidence for the spilling solitary to breaking bore hypothesis. Assuming that the waves with periods between five and ten seconds have larger deep water amplitudes than those with periods less than five seconds, then the longer period waves break in deeper water. Thus, by the time the larger waves pass the measuring position, they have transformed more than the smaller and shorter period waves.

The large standard deviation of U_r for the surf-bores is to be expected since all waves which were breaking when they passed the wave staff are included. Table IV shows h_1/h_2 and U_r for the surf-bores and undular surf-bores. Notice that the means and standard deviations of h_1/h_2 for the undular surf-bores are slightly lower, while their U_r values are somewhat greater. This is explained by the classification scheme. The surf bore data include all breaking waves except those in the undular surf-bore class; this includes fully developed surf-bores and breakers just shoreward of the incipient spilling stage. The undular surf-bore is a more restricted class; these waves should be relatively long (high U_r) with saw-toothed shaped profiles. In addition, they should have lower h_1/h_2 values since they are partly undular.

Prior to viewing the time-lapse photographs, it was thought that the interaction of large bores overtaking smaller bores would be recorded frequently. Actually very few of these bore-bore interactions occurred. However, on one occasion a large bore was observed to overtake and completely destroy a smaller bore; in this case Peregrine's

(1974) bore interaction theory could not be adequately tested.

In conclusion, these measurements support the spilling breaker-to-surf bore transformation hypothesis for waves on gently sloping beaches (s = 0.007) put forth by Huntley and Bowen (1975a). The low average value of the index h_1/h_2 (1.64) and its rather large standard deviation (0.2) for the breaking waves can be explained by the amplitude dispersion mechanism characteristic of finite amplitude long waves. These measurements suggest that previous studies assuming a constant H/h index (Longuet-Higgins, 1970; Bowen, Inman, and Simmons, 1968) across the width of the breaker and surf zones can be expected to be only partially correct. Within the surf zone, amplitude dispersion causes continual steepening and eventual breaking of the wave somewhat independently of the wave height to depth ratio.

Surf Zone Spectra

Power spectra were computed to investigate the range of frequencies greater than the lowest predominant incident wave frequency. Each time series consists of 4096 points spaced 0.20 seconds apart, and spectrum estimates are computed at 256 equally spaced frequencies between 0.0 $sec.^{-1}$ and 2.5 $sec.^{-1}$. These spectral estimates are the Gaussian weighted averages of nine frequency points (Appendix I and Borgman, 1972). Thus each average spectral estimate has 18 associated degrees of freedom, and the 80% confidence limits for each estimate are between 0.60 and 1.66 times the estimate.

The spectral energy density for five pairs of synoptic water surface elevation records at two surf zone locations are plotted in

Figure 20. The ordinate value 671. is a reference value; that is, for each pair of spectra the ordinate axis is shifted so this value is near the higher part of the spectrum. The vertical distance between the ordinate values 671. and 67.1 shows the ordinate log scale applicable to all 671. values.

The major characteristic of these spectra is the approximately linear decay on the semi-log scale of the energy with increasing frequency; only a few of the peaks are statistically significant according to the 80% confidence limits. These significant peaks occur in the period range 13.0 to 26.0 seconds. The significant energy density at the longer periods (26. sec.) may be due to breaker interactions of as yet an unspecified nature, since bore-bore interactions were only infrequently observed. Because the beach slope is small ($s = 0.007$), reflected long period swell and subharmonic edge waves are not likely candidates. Neither is swash-backwash interaction since the measurements were taken in the surf zone and not the swash zone.

Figure 21 shows the same characteristic for the spectra of the onshore-offshore current and surface elevation recorded simultaneously at the same location. However, the peak in the period range 13.0 to 15.0 seconds is especially pronounced.

The spectral energy densities between 0.076 $sec.^{-1}$ and 0.20 $sec.^{-1}$ ($T = 13.2$ sec. to 5.0 sec.) were replotted with a smaller frequency interval to discover (1) if the dominant incident wave frequency is detectable and (2) if there is a significant peak at the first harmonic of the incident wave frequency. The lower cutoff

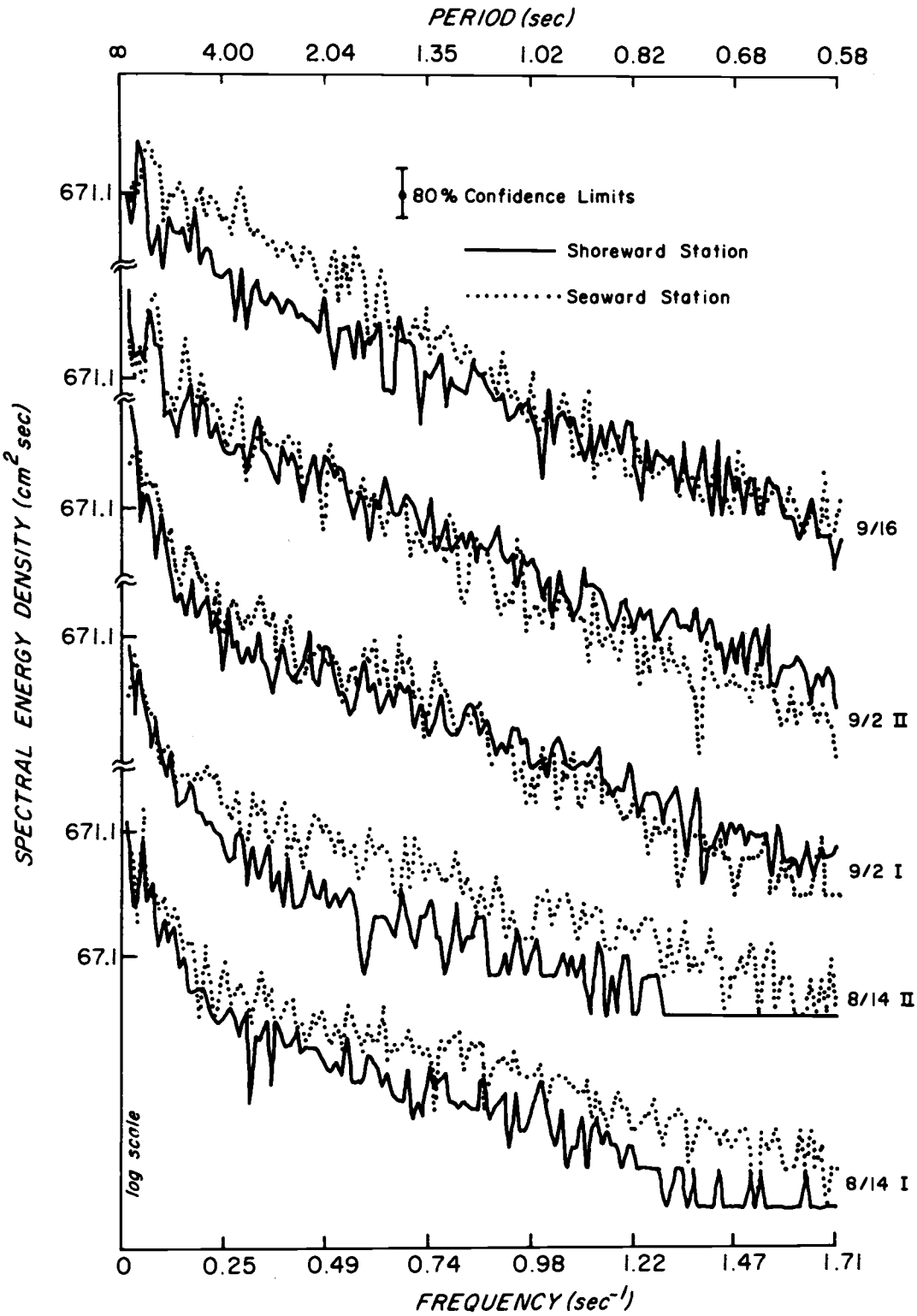

Figure 20. Spectral energy density of five pairs of surface elevation records measured simultaneously at two surf zone locations.

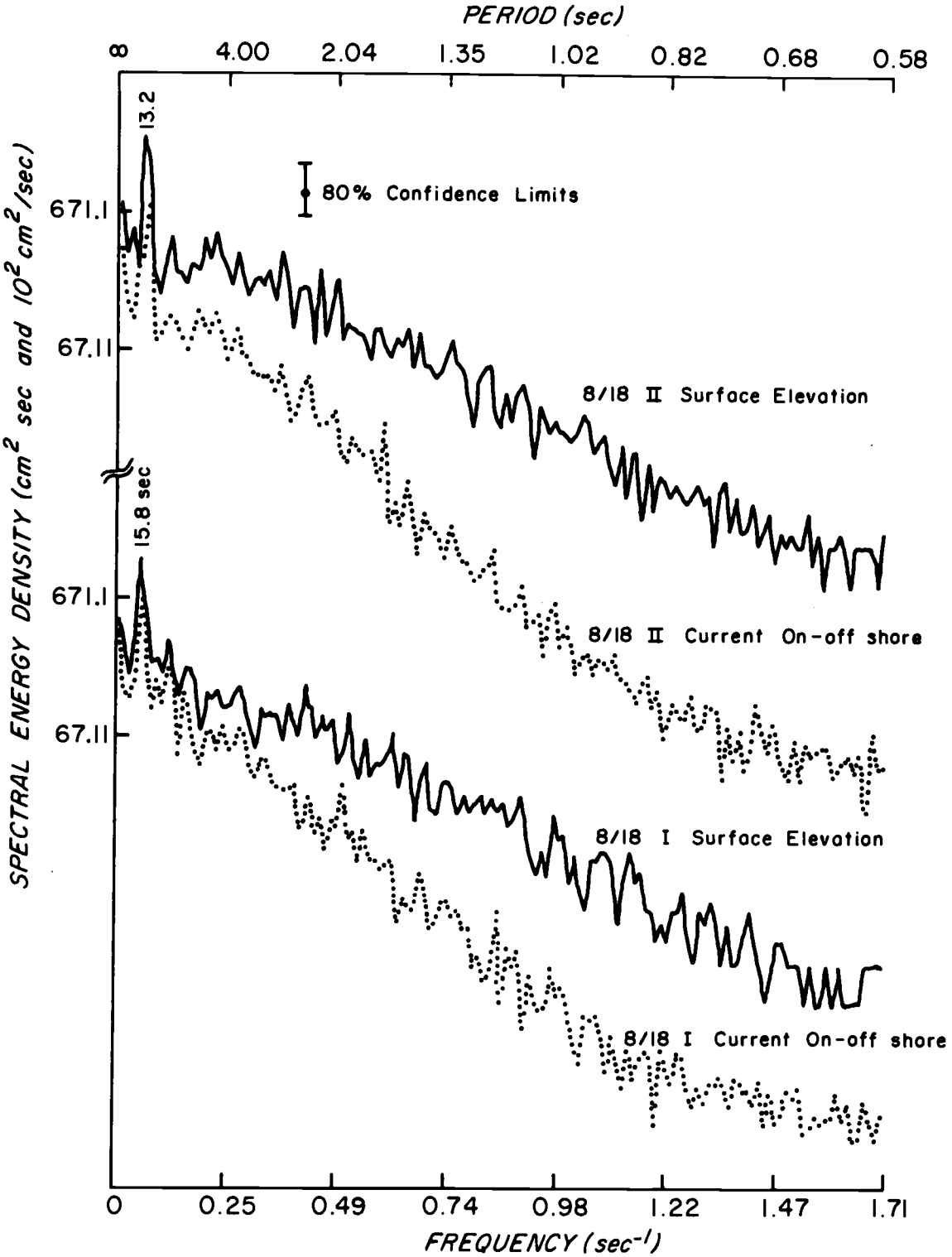

Figure 21. Spectral energy density of surface elevation and onshore-offshore orbital particle velocity recorded simultaneously at one surf zone location.

frequency (0.076 sec.$^{-1}$, or 13.2 sec.) is based on (1) the estimated generating wind field (less than 20 knots), (2) the significant wave height and period in deep water (Table II), and (3) co-cumulative spectra for various fetch and wind values published by Pierson, Neumann, and James (1960).

Figure 22 shows that the data identified as 9/2 II have a significant energy peak at about 0.08 sec.$^{-1}$ (11.8 sec.) at both the sea and shore staff positions; this peak is most likely due to the predominant incident waves. The shoreward location also has a statistically significant peak at about 0.15 sec.$^{-1}$ (6.7 sec), near the first harmonic (0.16 sec.$^{-1}$), while the seaward station does not. Most of the remaining spectra have such large variability in the frequency band 0.076 sec.$^{-1}$ to 0.09 sec.$^{-1}$ that it is difficult to detect significant peaks at the first harmonic of this band. It may be concluded that most of these spectral energy densities do not have a strong predominant peak. This explains the lack of a significant peak at the first harmonic of such a strong peak. A strong harmonic peak would be expected due to the saw-toothed asymmetry of the surf-bore profile.

Spectra of the surface elevation or the onshore-offshore orbital velocity in the surf zone ought to be a function of five variables, f, s, g, h, and $S_{bp}(f)$ in which $S_{bp}(f)$ is the spectral energy at the break point, and f is the frequency. S(f) depends on $S_{bp}(f)$ because $S_{bp}(f)$ determines H_b and h_b and thus the overall widths of the surf and breaker zones. The variation of S(f) with beach slope s has been well demonstrated by Huntley and Bowen (1975a). Although the beach slope is not varied in this study, it is retained as the effective

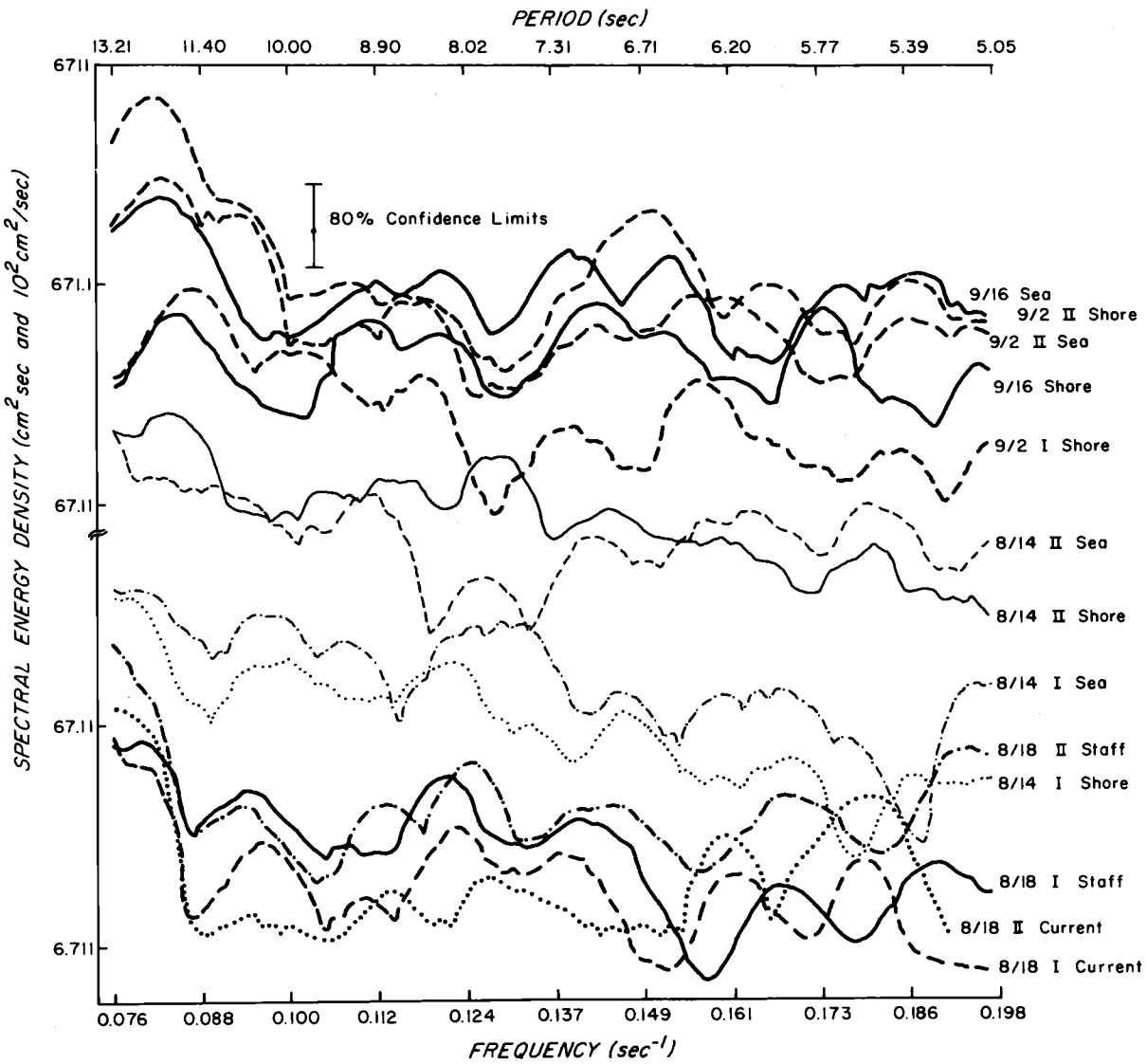

Figure 22. Spectra of Figure 20 in frequency band 0.076 sec.$^{-1}$ to 0.20 sec.$^{-1}$.

downslope gravity component; the incipient breaker type depends primarily on the beach slope (see part one of this thesis). The local depth h is a significant parameter effecting S(f) as indicated by the breaking index H/h.

An acceptable theoretical transformation relating $S_{bp}(f)$ to S(f) has not been derived. However, these five variables ought to a great extent determine this function. Unfortunately, the energy density at the break point $S_{bp}(f)$ was not measured so that it cannot be included in this analysis. To evaluate the dependence of S(f) on the remaining four variables, s, g, h, and f, f and S(f) are nondimensionalized. If the nondimensional variables are correctly chosen, the twelve different sets of data ought to fall on the same dimensionless curve. The nondimensional frequency chosen is $f' = f/(g/h)^{1/2}$, and the nondimensional spectral energy density is $S'(f) = S(f)\ (gs)^{1/2}/h^{2.5}$. Utilizing these forms smoothed spectra are plotted in Figure 23. A straight line is seen to form, approximately fitted by the equation

$$S'(f') = 0.0242 \exp(-13.15f') \qquad (23)$$

for $f' > 0.04$. Equation (23) may be rewritten in an equivalent form as

$$S'(f') = 0.0143 \exp(-13.15(f'-0.04)) \qquad (24)$$

where $S'(f' = 0.04) = 0.0143$. This form of S'(f') is a reminder that the nondimensional spectral maxima occurs at $f' = 0.04$. In all cases f' yields a dimensional frequency greater than the predominant incident wave frequency. Substituting the dimensional relationships for S'(f')

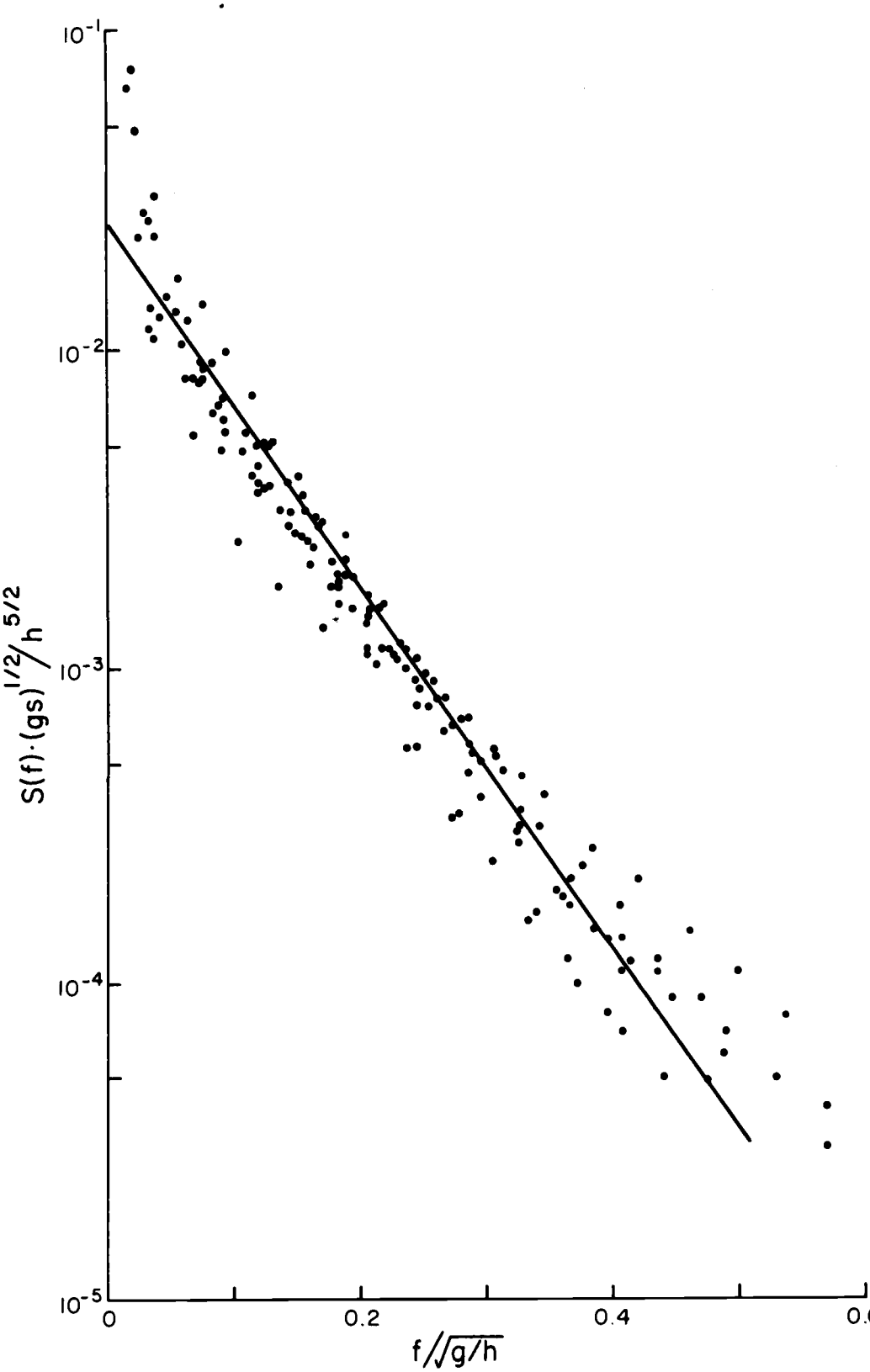

Figure 23. Nondimensional spectra of surface elevation measurements.

and f' into equation (24) yields

$$S(f) = \frac{0.0143\ h^{2.5}}{(sg)^{1/2}} \exp(-13.15(f-0.04(g/h)^{1/2})/(g/h)^{1/2}) \quad . \quad (25)$$

Huntley and Bowen (1975a) obtained a similar form for the onshore-offshore current velocity. However, the depth dependence of S(f) was limited to the argument of the exponential. Here it is reasoned that the maximum value of the spectral energy density ought to decrease with decreasing depth as the breaking waves travel shoreward, especially at frequencies above the predominant wave frequency.

In this equation the empirically determined constants (0.0143 and -13.15) must somehow be related to the spectral energy density at the breakpoint; a variable which was not measured. Further study of the functional dependence of S(f) on $S_{bp}(f)$ has not yielded an explanation for how these constants are related to $S_{bp}(f)$. In addition, the low cutoff frequency depends on the predominant incident wave frequency as shown by Figure 23.

CONCLUSIONS

Field measurements of surf-waves on a gently sloping beach (s = 0.007) support the following conclusions:

1. Waves in the surf zone can be classified broadly into four types with the surf-bore most typical (Figures 15 and 17); these waves have characteristic local surface profiles (Figure 16).

2. The surf-bore and the undular surf-bore are distinguishable from the non-breaking waves by the parameters h_1/h_2 and U_r (Tables III

IV), but not from each other. The term surf-bore, or breaking long wave, is appropriate because (a) h_1/h_2 averaged 1.64, lower than the theoretical value for maximum height solitary waves (1.8) and (b) its standard deviation (0.2) is large enough to reasonably conclude that many waves continue to break due to the amplitude dispersion mechanism characteristic of long waves. If amplitude dispersion is the important mechanism, then the breaking index H/h cannot be expected to be constant at either a fixed location in the surf zone or across the surf zone width.

3. The spectral energy density of the local surface elevation within the surf zone is approximately given by the equation

$$S(f) = \frac{0.0143\ h^{2.5}}{(gs)^{1/2}} \exp(-13.15(f-0.04(g/h)^{1/2})/(g/h)^{1/2}$$

for $f > 0.04(g/h)^{1/2}$. The constants (0.0143 and -13.15) are actually variables in that they are determined from the input spectral energy density which was nearly constant in the present study. In addition, the lower cutoff frequency is always greater than the predominant wave frequency.

4. Even though many individual surf-bore profiles show saw-toothed asymmetry, statistically significant spectral peaks at the harmonic frequency of the predominant waves were not pronounced.

BIBLIOGRAPHY

Bakhmeteff, B. A. and A. E. Matzke, The hydraulic jump in terms of dynamic similarity, Amer. Soc. Civil Engr., Transactions, 101, 630-680, 1936.

Biesel, F., Study of wave propagation in water of gradually varying depth, Gravity Waves, Circ., 521, Nat. Bur. of Stand., 243-253, 1952.

Binnie, A. M. and J. C. Orkney, Experiments on the flow of water from a reservoir through an open horizontal channel: the formation of hydraulic jumps, Proc. Roy. Soc., A, 230, 237-246, 1955.

Bodvarsson, G., Ocean wave-generated microseisms at the Oregon coast, Oregon State University, M.S. thesis, 83 numb. leaves, 1975.

Borgman, L. E., Confidence intervals for ocean spectra, Proc. 13th Conf. on Coastal Engr., 237-250, 1972.

Bowen, A. J. and D. L. Inman, Rip currents, laboratory and field observations, J. Geophys. Res., 74(23), 5479-5489, 1969.

Bowen, A. J., D. L. Inman, and V. P. Simmons, Wave set-down and set-up, J. Geophys. Res., 73(8), 2569-2577, 1968.

Camfield, F. E. and R. L. Street, Observations and experiments on solitary wave deformation, Proc. 10th Conf. Coastal Engr., 284-301, 1967.

Chow, V. T., Open-channel hydraulics, McGraw-Hill Co., 680 p., 1959.

Divoky, D., B. Le Mehaute, and A. Lin, Breaking waves on gentle slopes, J. Geophys. Res., 75(9), 1681-1692, 1970.

Emery, K. O. and J. F. Gale, Swash and swash mark, Trans., Amer. Geophys. Union, 32(1), 31-36, 1951.

Enfield, D. B., Prediction of hazardous Columbia River bar conditions, Oregon State University, Ph.D. thesis, 204 numb. leaves, 1974.

Favre, H., Etude theorique et experimentale des ondes de translation dans les canaux decouverts, Dunrod, Paris, 1935.

Gallagher, B., Some qualitative aspects of nonlinear wave radiation in a surf zone, J. Geophys., Fluid Dynamics, 3, 347-354, 1972.

Galvin, C. J., Jr., Breaker type classification on three laboratory beaches, J. Geophys. Res., 73(12), 3651-3659, 1968.

Galvin, C. J., Jr., Breaker travel and choice of design wave height, J. Waterways and Harbors Div., WW 2, 95, 175-200, 1969.

Gaughan, M. K., P. D. Komar, and J. H. Nath, Breaking waves: a review of theory and measurements, Oregon State University, School of Oceanography, Ref. 73-12, 145 p., 1973.

Henderson, F. M., Open channel flow, Macmillan Co., 522 p., 1966.

Ho, D. V., R. E. Meyer, and M. C. Shen, Long surf, J. Mar. Res., 21(3), 219-232, 1962.

Horikawa, K. and C. Kuo, A study of wave transformation inside the surf zone, Proc. 10th Conf. Coastal Engr., 217-233, 1967.

Huntley, D. A. and A. J. Bowen, Comparison of the hydrodynamics of steep and shallow beaches, In: Nearshore sediment dynamics and sedimentation, Eds. J. Hails and A. Carr, John Wiley and Sons, 69-109, 1975a.

Huntley, D. A. and A. J. Bowen, Field observations of edge waves and their effect on beach material, J. Geolog. Soc., Lond., 131, 69-81, 1975b.

Ippen, A. T. and G. Kulin, The shoaling and breaking of the solitary wave, Proc. 5th Conf. Coastal Engr., 27-49, 1955.

Ijima, T., M Takahiko, and K. Koga, Equilibrium range spectra in shoaling water, Proc. 12th Conf. Engr., 137-149, 1970.

Iversen, H. W., Studies of wave transformation in shoaling water, including breaking, Gravity Waves, Circ. 521, Nat. Bur. of Stand., 9-32, 1952.

Keulegan, G. H. and G. W. Patterson, Mathematical theory of irrotational translation waves, J. Res. of the Nat. Bur. of Stand., 24, 47-101, 1940.

Komar, P. D. and M. K. Gaughan, Airy wave theory and breaker height prediction, Proc. 13th Conf. Coastal Engr., 405-418, 1973.

Longuet-Higgins, M. S., Longshore currents generated by obliquely incident sea waves, 1, J. Geophys. Res., 75(33), 6778-6789, 1970.

Marsh, A. and W. McBirney, Operating and service manual for electromagnetic water current meter model 711, Marsh-McBirney, Inc., 2281 Lewis Ave., Rockville, MD., 1972.

Meyer, R. E. and A. D. Taylor, Run-up on beaches, In: Waves on Beaches, Ed. R. E. Meyer, Academic Press, 357-412, 1972.

Munk, W. H., Solitary wave theory and its application to surf problems, Ann. N. Y. Acad. Sci., 51, 376-424, 1949.

Nakamura, M., H. Shiraishi, and Y. Sasaki, Wave decaying due to breaking, Proc. 10th Conf. Coastal Engr., 234-253, 1967.

Peregrine, D. H., Water wave interactions in the surf zone, Proc. 14th Conf. Coastal Engr., 500-517, 1974.

Peregrine, D. H., Equations for water waves and the approximations behind them, In: Waves on Beaches, Ed. R. E. Meyer, Academic Press, 95-122, 1972.

Peregrine, D. H., Calculations of the development of an undular bore, J. Fluid Mech., 25, 321-330, 1966.

Pierson, W., G. Neumann, and R. W. James, Observing and forecasting ocean waves, U. S. Hydrographic Office Pub. 603, 284 p., 1955.

Sandover, J. A., and O. C. Zienkiewicz, Experiments on surge waves, Water Power, 9, 418-424, 1957.

Schiffman, A., Energy measurements in the swash-surf zone, Limnol. and Oceanogr., 10, 255-260, 1965.

Steer, R., Kinematics of water particle motion within the surf zone, Naval Postgraduate School, M.S. thesis, 56 numb. leaves, 1972.

Stoker, J. J., Water waves, Interscience Publ. Inc., 567 p., 1957.

Stolzenbach, K. D., Field evaluation of a bi-axial electromagnetic velocity probe, Conf. Internat. Assoc. for Hydraulic Res., Sao Paulo, Brazil, 10 p., 1975.

Suhayda, J. N., Standing waves on beaches, J. Geophys. Res., 79(21), 3065-3071, 1974.

Suhayda, J. N., and N. R. Pettigrew, Celerity of surf, Trans., American Geophys. Union, 56(12), 1136, 1974.

Ursell, F., The long wave paradox in the theory of gravity waves, Proc. Cambridge Phil. Soc., 49, 685-692, 1952.

Waddell, E., A field investigation of swash characteristics, J. Coastal Engr. in Japan, 16, 61-71, 1973.

Zabusky, N. J. and C. J. Galvin, Shallow water waves, the Korteweq-deVries equation and solitons, J. Fluid Mech., 47(4), 811-824, 1971.

APPENDIX

APPENDIX I

Spectral Energy Density Calculations

A subroutine named RCTFFT available in the Arand Time Series Subroutines Manual written by the Oregon State University Computer Center was used to calculate the Fourier coefficients of a series of real data points using a fast Fourier transform algorithm. The number of data points must be equal to two raised to an integer power.

If the number of real data points is 2N, let X(t), t = 0,1,.... ..,2N-1, be these points. The Fourier coefficients are the coefficients of the trigonometric series

$$X(t) = 1/2a(0) + \sum_{n=1}^{N-1} (a(n)\cos(2\pi tn/2N) + b(n)\sin(2\pi tn/2N)) + 1/2(-1)^t a(N)$$

for t = 0, 1,.....2N-1 and they are given by the expressions

$$a(n) = \frac{1}{N} \sum_{t=0}^{2N-1} X(t)\cos(2\pi tn/2N) \qquad n=0,1,..,N$$

$$b(n) = \frac{1}{N} \sum_{t=0}^{2N-1} X(t)\sin(2\pi tn/2N) \qquad n=1,2,..,N-1$$

The fast Fourier transform algorithm used to compute a(n) and b(n) is the Cooley-Tukey time decimation algorithm. The spectral energy density S(f) is computed from a(n) and b(n) according to the equation

$$S(f_n) = (a^2(f_n) + b^2(f_n)) / \Delta f$$

where $\Delta f = 1/2N\Delta t = 0.001221$ sec.$^{-1}$, $\Delta t = 0.20$ sec., $2N = 4096$, and $f_n = n/819.2$ (sec.$^{-1}$) for $n = 0,1,\ldots,2048$.

To smooth the raw spectral energy density estimates, a Gaussian weighted average of nine values is used (Borgman, 1972):

$$S_m^* = \left(\sum_{j=1}^{j=9} W_{m-j} \; S_j^* \right) / 9$$

where

$$W_{m-j} = \exp(-(m-j)\Delta f)^2/2p^2) \quad ,$$

$p = 3\,\Delta f$, and for N = 9 the weights are

$W_m = 1.0$

$W_{m-1} = W_{m+1} = 0.946$

$W_{m-2} = W_{m+2} = 0.801$

$W_{m-3} = W_{m+3} = 0.607$

$W_{m-4} = W_{m+4} = 0.414$